E&G Quaternary Sci. J., 75, 131–162, 2026
https://doi.org/10.5194/egqsj-75-131-2026

Open Access E&G Quaternary Science Journal

Research article

Review of numerical methods for dating Quaternary volcanism

William McCreary[1], **Venera May**[2], **Daniela Mueller**[1,3], **Elena Serra**[4], **and Frank Preusser**[1]

[1]Institute of Earth and Environmental Science, University of Freiburg, 79098 Freiburg, Germany
[2]School of Geography, Earth, and Atmospheric Sciences, University of Melbourne, Parkville, 3010, Australia
[3]School of Environmental Sciences, University of Liverpool, Liverpool, L69 7ZT, United Kingdom
[4]Institute of Earth Surface Dynamics, University of Lausanne, Lausanne, 1015, Switzerland

Correspondence: William McCreary (william.mccreary@geologie.uni-freiburg.de)

Relevant dates: Received: 18 December 2025 – Revised: 9 June 2026 – Accepted: 11 June 2026 – Published: 30 June 2026

How to cite: McCreary, W., May, V., Mueller, D., Serra, E., and Preusser, F.: Review of numerical methods for dating Quaternary volcanism, E&G Quaternary Sci. J., 75, 131–162, https://doi.org/10.5194/egqsj-75-131-2026, 2026.

Abstract: The quality of the numerical age estimates used to establish the eruption chronology of a volcanic field is a critical control on the dependability of temporal hazard assessments. However, researchers involved in hazard assessment and modelling may be unfamiliar with dating methods and their complexities, which are needed to assess the quality of published ages. This paper aims to increase the awareness regarding the quality of geochronological data by providing brief introductions to the principles and applications of the dating methods applicable to Quaternary volcanism. The numerical dating methods included in this review are as follows: ^{40}K / ^{40}Ar and ^{40}Ar / ^{39}Ar dating, radiocarbon dating, uranium-series-related dating, cosmogenic nuclide exposure dating, and luminescence dating, as well as tephrostratigraphy and annual layer counting. First, the physical phenomena utilised by each method to provide age estimates are presented and then concerns related to the application of these methods are discussed, including necessary calibration steps and possible sources of error. This is followed by examples of the application of each of the methods.

Kurzfassung: Die Qualität numerischer Altersabschätzungen, die für zeitliche Einordnung von Ausbrüchen eines Vulkanfeldes genutzt werden, spielt eine kritische Rolle für die Zuverlässigkeit der zeitlich-aufgelösten Gefährdungsbeurteilung. Oft fehlt Forschenden, die in die Gefährdungsbeurteilung und -modellierung involviert sind, ein eingehendes Verständnis für die genutzten Datierungsmethoden und deren Komplexität. Dieses Verständnis ist jedoch Voraussetzung, um die Qualität publizierter Alter einschätzen zu können. Die vorliegende Arbeit soll das Bewusstsein bezüglich der Qualitätsfaktoren geochronologischer Daten schärfen, indem die Prinzipien und Anwendungen von Methoden zur Datierung quartären Vulkanismus zusammenfassend vorgestellt werden. Hierbei handelt es sich um Datierungsmethoden mittels ^{40}K / ^{40}Ar und ^{40}Ar / ^{39}Ar, Radiokohlenstoff, Uranzerfallsreihen, kosmogener Nuklide und Lumineszenz, sowie Tephrastratigraphie und Zählung von Jahreslagen. Zuerst werden die physikalischen Hintergründe der einzelnen Methoden vorgestellt. Im Anschluss werden Probleme bei der Anwendung diskutiert, inklusive notwendiger Schritte zur Kalibrierung und potentielle Fehlerquellen diskutiert und Anwendungsbeispiele vorgestellt.

Published by Copernicus Publications on behalf of the Deutsche Quartärvereinigung (DEUQUA) e.V.

1 Introduction

Volcanism is widespread across the Earth in a variety of forms. In many cases human societies have developed near volcanoes, often due to benefits such as fertile soil (Small and Naumann, 2001). Proximity to volcanoes, however, comes with the hazard of periodic sudden destruction from ballistic projectiles, ashfall, pyroclastic surges, lava flows, and lahars. An understanding of the time frame and recurrence rate of volcanic activity is critical for assessing the risk posed by these volcanic hazards. Forecasting the risk of these hazards is of particular concern to urban areas located near or within volcanic fields such as Auckland (New Zealand), Mexico City (Mexico), Naples (Italy), and Clermont-Ferrand (France). Furthermore, long-term forecasting of volcanism is necessary for critical decisions such as the locations of nuclear waste repositories (e.g. Connor et al., 2000).

To consider the temporal element of hazard forecasting, the sequential eruption order and the ages of the eruptions are needed. From this information, the recurrence rate of eruptions, i.e. the duration of time between successive eruption events, can be calculated. Numerical age estimations for individual eruptive centres are thus crucial for long-term temporal eruption forecasting. Unfortunately, most volcanoes lack chronologic data, or the available data are of questionable quality (Le Corvec et al., 2013). For example, a survey of the southwestern USA found that out of over 2000 identified Quaternary volcanoes, in 37 distinct fields, only around 25 % have been dated (Valentine et al., 2021). While this percentage might seem low, it is relatively good on a global scale, with many Quaternary volcanic fields for which barely any eruption chronologies exist (Brown et al., 2015). Furthermore, many ages are published without analytical information or error estimates, and/or were determined using older dating methods that have been found to be erroneous. These are factors that considerably affect the reliability of the age estimates and that of the calculated recurrence intervals between eruption events.

As most researchers who use chronological information for further analysis, including those interested in forecasting volcanic hazards, may not be familiar with geological dating methods, the objective of this paper is to provide a brief introduction to the methods currently available for dating volcanic eruptions. Extra attention is given to common problems encountered with these methods and special considerations that may be needed in volcanic settings. We will focus on numerical dating methods available for volcanic products of Quaternary age, as these are the most pertinent for hazard assessments. Additionally, the temporal record of volcanic products is skewed towards younger epochs due to the erosion potential of their landforms. Our intention is that readers will become familiar with the dating tools available to them for future campaigns and will be able to evaluate the reliability of existing ages.

2 Dating Quaternary volcanism

The dating methods presented in this review are applicable to all kinds of volcanism, on the condition that suitable sample materials are produced. To facilitate the discussion of the full range of methods, dispersed volcanism and the resulting volcanic fields will be the focus of this review. This is due to the diversity of landforms and volcanic products associated with volcanic fields (Fig. 1). These landforms are generally the result of a single small batch of magma (typically $< 1\,km^3$) ejected through a simple conduit during a single short ($< 100\,a$) eruption period (Cañón-Tapia, 2016; Smith and Németh, 2017). Each batch of magma ascends along a new conduit to erupt at a new location, thus building a spatially distributed field of volcanoes. Each of these individual systems operates on its own timescale but is likely influenced by the dynamics of the greater system. While the eruption of an individual volcano in a field is short, the lifetime of a field may span millions of years, even exceeding the lifetime of composite volcanoes (Nemeth, 2010). Volcanic fields pose an increased hazard risk because of their dispersed nature; each new eruptive centre will erupt in a new location. Thus, spatiotemporal models of activity for the entire volcanic field are needed for hazard forecasting (Valentine and Connor, 2015).

In this review, the numerical dating methods most used for Quaternary volcanism are presented (Fig. 2). We refrain from discussing relative and maximum semi-quantitative approaches such as morphometric analysis (e.g. Vörös et al., 2021, 2022). We also refrain from discussing approaches based on utilising changes in the magnetic field of the Earth, as these do not directly provide numerical ages and have recently been reviewed by others (Ort et al., 2015; Lerner et al., 2022). The numerical methods presented are all based on phenomena either directly or indirectly related to radioactivity and nuclear physics. This is because radioactive decay is one of the few natural processes occurring at constant rates over geological timescales. Four out of the six methods directly date volcanic products: potassium/argon ($^{40}K / ^{40}Ar$) and argon/argon ($^{40}Ar / ^{39}Ar$) dating, uranium-series-related dating (U-series), cosmogenic nuclide exposure dating, and luminescence dating. In contrast, radiocarbon dating is used to date organic material found within volcanic deposits or to provide maximum and minimum ages for eruptions by dating organic material bracketing volcanic deposits.

Volcanoes produce a variety of deposits and landforms that can be used for dating (Fig. 1). Scoria cones and lava flows are locations where sample materials like massive lava for $^{40}K / ^{40}Ar$ and $^{40}Ar / ^{39}Ar$, U-series dating, and cosmogenic nuclide exposure dating can be found. In, and under, lava flows it is also possible to find organic material burnt

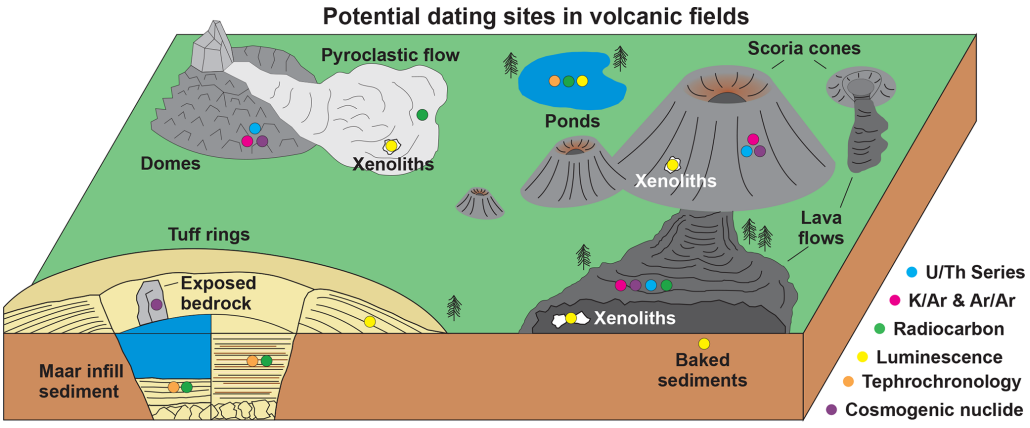

Figure 1. General schematic of a volcanic field and the related landforms. Locations where potential samples for dating can be found are indicated by the coloured dots.

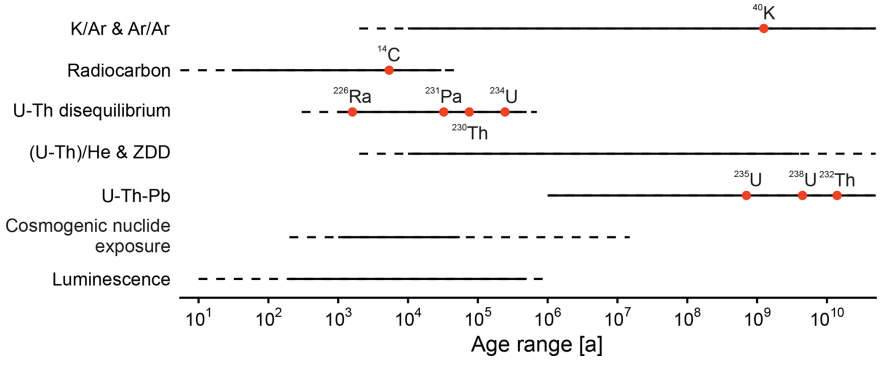

Figure 2. Applicable dating ranges for the methods covered in this review presented as bars on a logarithmic scale. Dashed portions of the bars represent ranges where ages should be approached with caution. The red points indicate the half-life of the associated isotope in relationship to the dating range.

by the lava that can be dated through radiocarbon methods. More evolved magmas with trachytic and rhyolitic compositions produce lava domes and pyroclastic flows, which can be dated through U-series, cosmogenic nuclide exposure, and ^{40}K / ^{40}Ar and ^{40}Ar / ^{39}Ar methods, depending on the mineralogical composition of the resulting lavas. Pyroclastic surge deposits also potentially contain organic material that was present in the path of the surge during eruption and was picked up by the flow. Later deposited, these can be dated through radiocarbon methods. Other locations where sample material for dating measurements can be found are at quarries, roadcuts, pond sediment cores (both proximal and distal), and the sediment infill of maar or tuff ring craters. Exposed rock faces in these craters can also be dated through cosmogenic nuclide exposure dating to provide a formation age for the maar or tuff ring.

The components of the deposits described in the previous paragraph can be divided into three main categories: juvenile, accessory, and accidental. Juvenile components are those that solidify directly from magma, including lava and tephra fragments erupted into the air. As all magmas are only partially melt, juvenile rocks will be composed of phenocrysts – crystals formed from the melt – surrounded by a glassy matrix representing the melt at the time of eruption. Silicate minerals crystallise out of a melt based on their individual phase dynamics in a sequence known as Bowen's reaction series (Bowen, 1922). This series starts with minerals rich in iron and magnesium (olivine and pyroxene), and ends with pure silica oxide (quartz). A side branch of this reaction series describes the crystallisation sequence of feldspars from calcium (Ca)-rich feldspar to sodium (Na)-rich and finally potassium (K)-rich feldspar. In addition to these main mineral phases, small amounts of minor minerals like zircon and apatite also crystallise from the melt. The lavas resulting from various melts follow a similar pattern: the initial lavas from unevolved magmas, such as basalt, are rich in iron and magnesium, while more evolved (i.e. differentiated) magmas produce silica-rich lavas like trachyte and rhyolite. The juvenile components of volcanic deposits are the target dating material for ^{40}K / ^{40}Ar and ^{40}Ar / ^{39}Ar, U-series, and, to some extent, cosmogenic nuclide exposure and luminescence dating. Accessory components are rocks

or minerals of non-volcanic origin that are brought to the surface during an eruption. This category includes xenoliths, fragments of the magma chamber or conduit walls that broke off and were subsequently transported to the surface during an eruption. These xenoliths experience various degrees of thermal alteration while entrained in the magma. They can often be found inside volcanic bombs or in lava flows (Fig. 1) and can be used as sample material for luminescence dating. Accidental components are rock fragments or minerals that have no relation to the magma but rather were incorporated into a volcanic deposit during explosive activity. These accidental components are particularly common in deposits from phreatic eruptions and can be found in tuff rings where they can potentially be used as sample material for luminescence dating.

There are two issues that affect all the dating methods presented in this section: proper age reporting and the reference datum. The question of how ages should be correctly reported remains unresolved between the different dating communities. As explained further below, age determinations are mainly based on applying rather complex approaches with many pitfalls. Advances in technology and analytical procedures have led to improvements regarding the precision, i.e. the reported age uncertainties, and the accuracy of the results (see Schoene et al., 2013). The latter stands for how close a reported age represents the real age of a deposit or an event. Systematic offsets between the apparent and real age are mainly not known (if known, one could usually correct for the reason), hence, even an age reported with a high precision might not necessarily be correct. To allow specialists to evaluate the quality of a result and identify potential problems, detailed reporting of sampling, analytic procedures, and the equipment used is required. Making this information available may allow corrections to be carried out, even decades after the information was initially published. Guidelines exist for most of the methods presented here (radiocarbon: van der Plicht and Hogg, 2006; Millard, 2014; ^{40}Ar / ^{39}Ar: Renne et al., 2009; U-series: Dutton et al., 2017; cosmogenic nuclides: Dunai and Stuart, 2009; luminescence: Mahan et al., 2022).

The other issue is the reference datum, as there is no common fixed year of reference. For most methods, the age reported refers to the year of sampling or measurement, which is not necessarily reported in the related studies. The radiocarbon dating community has defined 1 January 1950 as "present", and ages are usually reported as "BP" ("before present"; see van der Plicht and Hogg, 2006). When reporting ages for Pleistocene eruptions, this issue is secondary considering the overall range of dating uncertainties, but it becomes relevant on historic timescales (see Duller, 2011). A common solution to make ages comparable between methods is to use the AD/BC (Anno Domini/Before Christ) or CE/BCE (Common Era/Before Common Era) scale. However, converting ages to this scale requires that the reference year is properly reported. Finally, there is no consensus regarding the abbreviation with which ages are reported. Commonly found are "y", "yr", "yrs" (for years) but, more recently, many journals (e.g. Grün, 2008) follow The International System of Units (SI) and use the "a" (lat. annum = year), in combination with prefixes k (kilo = one thousand), M (mega = one million), and G (giga = one billion).

3 ^{40}K / ^{40}Ar and ^{40}Ar / ^{39}Ar dating

Both ^{40}K / ^{40}Ar and ^{40}Ar / ^{39}Ar dating methods are based on the radioactive decay of potassium-40 (^{40}K) to the stable noble gas argon-40 (^{40}Ar) in potassium-bearing minerals. In 1940, this decay was first utilised for chronological purposes (Aldrich and Nier, 1948), constituting the beginning of the ^{40}K / ^{40}Ar dating method. When minerals are held at elevated temperatures, gases such as Ar are purged from the mineral. After a K-bearing mineral cools, gaseous ^{40}Ar produced by the decay of ^{40}K (half-life ($t_{1/2}$) = 1250 Ma) becomes trapped within the crystalline lattice. As the decay of ^{40}K occurs at a constant rate, the ratio of ^{40}Ar to ^{40}K provides an indication of the time elapsed since the mineral cooled below a closure temperature. This closure temperature is dependent on diffusion processes in crystals, which in turn vary with mineral type, cooling rate, compositional variation, and structural state. It is better considered as a closure temperature range, with high cooling rates resulting in higher and narrower ranges, while slower cooling rates result in lower and broader temperature ranges (Snee, 2002). Closure temperature ranges are approximately 580 to 480 °C for amphibole (Harrison, 1982), 340 to 280 °C for biotite (McDougall and Harrison, 1999), and ≥ 300 to ≤ 150 °C for K-feldspar (McDougall and Harrison, 1999), with the upper and lower limits representing fast (1000 °C Ma^{-1}) and slow (5 °C Ma^{-1}) cooling rates, respectively. To overcome issues inherent to ^{40}K / ^{40}Ar dating (discussed in greater detail below), Merrihue (1965) and Merrihue and Turner (1966) developed the method known as ^{40}Ar / ^{39}Ar dating. Both methods are still in use today, often in tandem, and are particularly applicable to the dating of lava.

3.1 Procedures, problems, and applications

^{40}K / ^{40}Ar and ^{40}Ar / ^{39}Ar dating methods both target K-rich sample materials. They are performed on whole-rock samples, groundmass, and individual phenocrysts. Due to the long half-life of ^{40}K, these methods can provide ages for rocks as old as 3 to 4 Ga (Kelley, 2002). The younger limit of ^{40}K / ^{40}Ar can be estimated at ∼ 1.5 ka, as the analytical precision of the method decreases and the errors associated with the age are large (Scaillet and Guillou, 2004). The type of material being dated has an impact on this younger limit of dating. Low-K feldspars, such as plagioclase, would produce larger uncertainties and thus an older minimum age limit, while sanidine (a high-K feldspar) would tend to result in better analytical precision and can provide younger ages.

One of the additional sources of uncertainty with $^{40}K / ^{40}Ar$ dating is that these two elements (^{40}K and ^{40}Ar) are in different physical states: solid and gas. Therefore, two aliquots of the sample are measured separately at different facilities, leading to biased results in non-homogeneous samples. Flame photometry, isotope dilution, or atomic absorption spectrometry are used to measure K, while the Ar isotope ratios are measured through mass spectrometry (Kelley, 2002). The $^{40}Ar / ^{39}Ar$ dating method was developed to avoid the need to measure two aliquots of sample. This approach converts ^{39}K to ^{39}Ar by neutron irradiation at a nuclear reactor and then measures all the different isotopes of Ar simultaneously with mass spectrometry (Merrihue and Turner, 1966). This indirect way of measuring ^{40}K through $^{39}Ar_K$, with the K subscript denoting the K origin, is feasible, as the natural abundance of all K isotopes is well known and does not change: $^{39}K = 93.2581\,\%$, $^{41}K = 6.7302\,\%$, and radioactive $^{40}K = 0.0117\,\%$.

By measuring the Ar isotopes, the ratio between radiogenic ^{40}Ar (designated $^{40}Ar^*$) and ^{39}Ar produced by neutron irradiation ($^{39}Ar_K$) can be calculated. This ratio is proportional to $^{40}Ar^* / ^{40}K$ and is further related to the $^{40}K / ^{40}Ar$ age of the rock (McDougall and Harrison, 1999). The age is calculated by comparing the $^{40}Ar^* / ^{39}Ar_K$ of the sample to that of a standard of well-known age. This standard should be irradiated simultaneously with the sample to determine the neutron flux received by the sample. The standard is thus called the neutron flux monitor and is used to calculate the "J parameter", which is dependent on the duration of irradiation, the neutron flux, and the neutron cross-section (Mitchell, 1968). Ages can finally be calculated for the sample through Eq. (1):

$$t = \frac{1}{\lambda} \ln\left[1 + J\frac{^{40}Ar^*}{^{39}Ar_K}\right], \quad (1)$$

where t is the age (in a), λ is the total ^{40}K decay constant ($5.54 \times 10^{-10}\,a^{-1}$), and J is the previously described J parameter.

Early $^{40}Ar / ^{39}Ar$ dating utilised a method in which the sample was completely fused, meaning all gases were released and analysed simultaneously, without the possibility of identifying samples that were thermally disturbed after crystallisation. Turner et al. (1973) proposed a dating protocol with step heating, representing a breakthrough for identifying thermal disturbances in the crystallisation history of a sample. Accordingly, an ideal sample produces the same age (within error) during all the heating steps, constituting what is known as a "plateau age". Examples of ideal and problematic samples can be found in Fig. 3a, b. The plateau age can be resolved using at least three contiguous heating steps which together represent more than 50 % of the total ^{39}Ar released (McDougall and Harrison, 1999).

Two of the main assumptions in $^{40}Ar / ^{39}Ar$ dating are that the system has remained closed since eruption, meaning negligible loss of ^{40}Ar to weathering or thermal alteration, and the absence of inherited ^{40}Ar from xenoliths. These assumptions can be evaluated through petrographic observation of the sample. Another important assumption is that all the measured ^{40}Ar is derived from ^{40}K decay (McDougall and Harrison, 1999). ^{40}Ar is the most abundant isotope of argon and is thus also abundant in the atmosphere. Therefore, the total ^{40}Ar measured in a rock or mineral can potentially have both a radiogenic ($^{40}Ar^*$) and an atmospheric ^{40}Ar component. The $^{40}Ar / ^{39}Ar$ method overcomes this problem by measuring ^{36}Ar and calculating the atmospheric $^{40}Ar / ^{36}Ar$ ratio, which is then compared to the present-day $^{40}Ar / ^{36}Ar$ value of 295.5 ± 0.5 (Nier, 1950). However, during the irradiation process, ^{36}Ar isotopes can be produced from calcium (Ca); hence, the $^{40}Ar / ^{36}Ar$ ratio alone is not a reliable solution. An additional isotope, ^{37}Ar (a non-naturally occurring isotope also produced from irradiation of Ca), must be measured to account for the ^{36}Ar produced by irradiation from Ca (McDougall and Harrison, 1999).

After measuring the Ar isotopes and applying corrections to ^{40}Ar and ^{36}Ar, several argon isotopic ratios can be derived such as $^{36}Ar / ^{40}Ar$ and $^{39}Ar / ^{40}Ar$. An isochron diagram plots the isotopic ratios from the individual heating steps in a binary plot (Fig. 3c, d). A regression line is fitted to these ratios, with the y intercept constituting the air composition. The air composition ratio ideally should be within error of the reciprocal of $^{40}Ar / ^{36}Ar = 295.5 \pm 0.5$, the present-day ratio (Nier, 1950). The x-intercept value is related to the amount of radiogenic argon, which is proportional to the age of the sample.

One additional consideration for $^{40}Ar / ^{39}Ar$ dating is the loss of ^{39}Ar through atomic recoil during irradiation. This phenomenon occurs when the momentum from the conversion of ^{39}K to ^{39}Ar displaces the ^{39}Ar atom by up to 0.08 µm, potentially releasing it from the crystalline lattice (Turner and Cadogan, 1974). This effect, which results in an age overestimation, is most significant on fine-grained sample materials (e.g. clay) where there is the greatest potential for recoil to result in the escape of ^{39}Ar (Kelley, 2002).

3.2 $^{40}K / ^{40}Ar$ and $^{40}Ar / ^{39}Ar$ dating in volcanic contexts

In the volcanic context, radiogenic ^{40}Ar accumulates in cooled volcanic products, particularly in massive lava and the crystal components of ash. These methods are important for dating volcanic deposits due to the long half-life of ^{40}K (1250 Ma) and the high abundance of K-rich minerals in several volcanic deposits. The $^{40}Ar / ^{39}Ar$ step heating technique is applied to K-bearing minerals in lava and is a reliable tool for dating eruptions.

Due to an observed tendency for anomalously high levels of atmospheric ^{40}Ar, caution should be exercised when dating ignimbrites, altered lavas, and glasses (Chernyshev et al., 2006). When dating whole-rock lava or groundmass

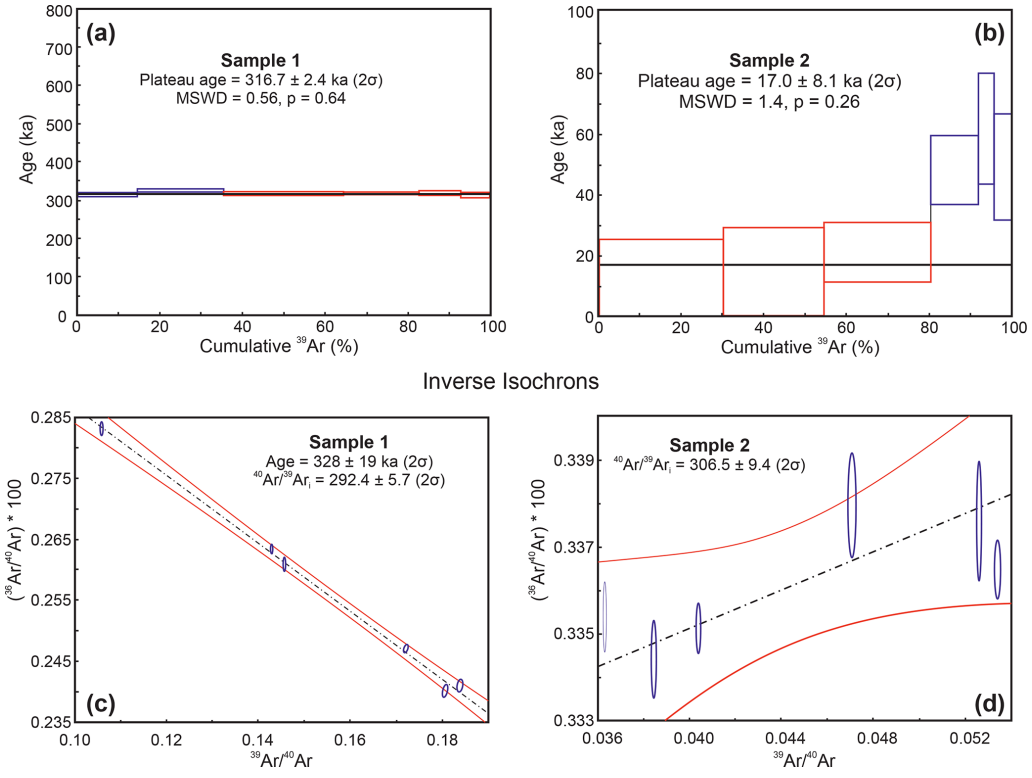

Figure 3. ^{40}Ar / ^{39}Ar step heating spectra results **(a, b)** and inverse isochrons **(c, d)** for two basalt samples from lava flows in the Payenia Basaltic Province, Argentina. Heating steps contributing to the plateau are shown in red and rejected steps in blue. Sample 1 shows all heating steps in agreement **(a)** and a well-defined isochron **(c)**, while sample 2 shows a deviation in the higher temperature heating steps **(b)** and a poorly defined isochron **(d)** (modified from May et al., 2018).

samples, special pre-treatment steps may be needed to remove phenocrysts and xenocrysts that could contain inherited ^{40}Ar (Guillou et al., 1998). Issues with atomic recoil of ^{39}Ar have also previously been documented for samples of basaltic lava (Baksi, 1994; Féraud and Courtillot, 1994). Nonetheless, approaches have been developed that allow reasonable ages to be calculated for basaltic samples that display nuclear recoil (Fleck et al., 2014). In recent years, a few approaches have been explored to extend the capabilities of the method and improve its precision. One example of this is improvements in analytical instrumentation through ultra-high-precision multi-collector mass spectrometers (Phillips and Matchan, 2013; Phillips et al., 2017). New methodologies such as single-grain age determination and using statistics to determine a normal distribution of ages have also been developed (Savelkouls et al., 2026; Schaen et al., 2020). However, performing single-grain ^{40}Ar / ^{39}Ar chronology requires a good understanding of the grain's history. Despite these advances, the problem of accurately dating young basaltic material remains.

3.3 Examples of ^{40}K / ^{40}Ar and ^{40}Ar / ^{39}Ar dating applied to volcanism

^{40}K / ^{40}Ar and ^{40}Ar / ^{39}Ar dating methods have been widely applied to the dating of lava flows. An example is the dating of nine lava flows in the Payenia Basaltic Province in central western Argentina by May et al. (2018). These lava flow samples were collected from fresh-looking basaltic flows. Two of the samples, sample 1 and sample 2, will be discussed further. Whole-rock samples of the basalt were crushed, and careful steps were taken to completely remove phenocrysts and xenocrysts from the sample. After irradiation, the Ar isotopes were measured through six heating steps. As shown in Fig. 3a, the step heating of sample 1 produced reliable results with a defined plateau. In addition, the inverse isochron graph (Fig. 3c) associated with sample 1 presents a (^{40}Ar / ^{36}Ar$_i$) value of 292.4 ± 5.7 (2σ), which is within error of the atmospheric value (295.5 ± 0.5; Nier, 1950), emphasising the reliability of the results (May et al., 2018). However, the step heating results for sample 2 (Fig. 3b) indicate that it is possibly very young and close to the younger limit of the method for basic volcanic material. This interpretation is determined from four factors: (a) the plateau age could only be derived from three consecutive heating steps, which is not ideal; (b) the resolved age presents a large error; (c) the

inverse-isochron-constrained $^{40}Ar / ^{36}Ar_i$ value is imprecise: 288.2 ± 23.3 (2σ) presenting a large uncertainty (Fig. 3d); and (d) the possibility of excess argon cannot be discarded.

Another example of the improvements presented by $^{40}Ar / ^{39}Ar$ dating in comparison to $^{40}K / ^{40}Ar$ dating is the research from Matchan and Phillips (2011) on the Newer Volcanic Province in southeastern Australia. Basalt samples were extracted from lava flows around Mount Rouse and Mount Warrnambool that had previously been studied with $^{40}K / ^{40}Ar$ dating (McDougall and Gill, 1975; Gill, 1981). Like the previous example, careful steps were taken to avoid rock fragments that were altered or contained phenocrysts and xenocrysts that may introduce excess Ar. The Ar isotopes were measured through seven steps of heating tailored to fit the individual samples. The $^{40}Ar / ^{39}Ar$ ages were mostly concordant with the previous $^{40}K / ^{40}Ar$ ages; however, the newer $^{40}Ar / ^{39}Ar$ chronology produces more precise results. Some of the $^{40}Ar / ^{39}Ar$ ages were found to be significantly younger than the $^{40}K / ^{40}Ar$ ages, which demonstrates the ability of $^{40}Ar / ^{39}Ar$ dating to avoid issues with excess Ar.

A final example of $^{40}Ar / ^{39}Ar$ dating that displays the limits of this method is the dating of Mt. Vesuvius deposits by Renne et al. (1997). These authors sampled pumice from deposits associated with the 24 August 79 CE eruption documented by Pliny the Younger. In contrast to the previous two examples, instead of dating the groundmass of basaltic lava, they targeted millimetric sanidine phenocrysts from the alkaline pumice. After irradiation, the sanidine crystals were step-heated with a broad-beam CO_2 laser. Despite showing dispersed ages in the lowest energy steps, in the higher energy steps an age from 2 to 3 ka emerged. When plotted on an isochron diagram, these data produced an age estimate of 1.925 ± 0.094 ka. Using the publication year, 1997, as the reference year, this age agrees well with the historically recorded age. Despite this positive result, there were clear indications of excess Ar in the sample, particularly in the lower steps. Nonetheless, attempts to correct for this excess by excluding the first two heating steps resulted in the indistinguishable age estimate of 1.927 ± 0.102 ka. This example shows that with careful application, modern $^{40}Ar / ^{39}Ar$ approaches can successfully be used to date late Holocene deposits.

4 Radiocarbon dating

Radiocarbon dating is based on the phenomenon of organic substances incorporating the radioactive isotope ^{14}C into their tissue during their lifetime (for reviews, see Hajdas, 2008; Hajdas et al., 2021; Wood, 2015). Upon the demise of the organism, the uptake of ^{14}C stops and those isotopes present in the remnants decay to ^{14}N with a half-life of 5.73 ka. As a result, the ratio of ^{14}C to the stable isotope ^{12}C within a sample will continuously decrease. By measuring and analysing the ratio of parent to child isotope, the time elapsed since the organism died, and thus the age of the deposit, can be determined. One of the most important breakthroughs in geochronology was the publication by Libby et al. (1949), which first presented age estimates based on the radiocarbon content of a sample.

4.1 Procedures, problems, and applications

Two different approaches exist to measure the concentration of ^{14}C in a sample. Originally, this was done by beta counting, i.e. using devices that measure the number of β particles emitted by radioactive decay of a sample. In the literature, this method is sometimes referred to as "conventional" radiocarbon. A relatively large amount of sample material (some grams) is required for this method, and for one sample it usually takes days of measurement to obtain robust counting statistics. The introduction of accelerator mass spectrometry (AMS) in the late 1970s revolutionised radiocarbon dating (Muller, 1977), as much smaller samples can now be measured at high levels of precision ($< 1\,\%$) in a few minutes (Linick et al., 1989). As 50 % of the ^{14}C remaining in the sample has decayed after each half-life, the detection limit is reached after approximately 10 half-lives, with only 0.1 % of the original ^{14}C remaining. Consequently, the upper limit for radiocarbon dating is around 55 ka (Hajdas et al., 2021). This 55 ka upper limit of radiocarbon dating is also practically established by the extent of the available calibration curves (discussed below). Radiocarbon ages as young as a few decades can be determined for certain material (see review by Geyh, 2001). However, it must be highlighted that caution is required in the sampling, storage, and preparation of samples to avoid contamination (e.g. Wohlfarth et al., 1998). This applies to bone material (e.g. Cersoy et al., 2017; Talamo and Richards, 2011) and especially for old samples (> 30 ka), as contamination can easily lead to offsets of several thousand years.

A general issue in radiocarbon dating is the fact that the primary production of the isotope ^{14}C in the atmosphere has not been constant over the last 55 000 a. This requires the radiocarbon age determined in the laboratory to be calibrated using atmospheric ^{14}C production rate curves that have been constructed from independently dated archives (Fig. 4). The establishment of such calibration curves began with Stuiver et al. (1986a), and the present curves cover a range from 0 to 55 000 cal BP (Heaton et al., 2020; Hogg et al., 2020; Reimer et al., 2020). These curves are based on tree rings with annual to decadal precision ages up to ~ 13.9 ka. Above this age, the curves are based on floating tree-ring chronologies, varved lake sediments, speleothems, ice core data, marine sediments, and corals. Because ^{14}C production is not uniform globally, separate curves have been established by international efforts for the Northern (IntCal20; Reimer et al., 2020) and Southern Hemispheres (SHcal20; Hogg et al., 2020). It has also been necessary to establish a calibration curve for marine samples due to differences in atmospheric

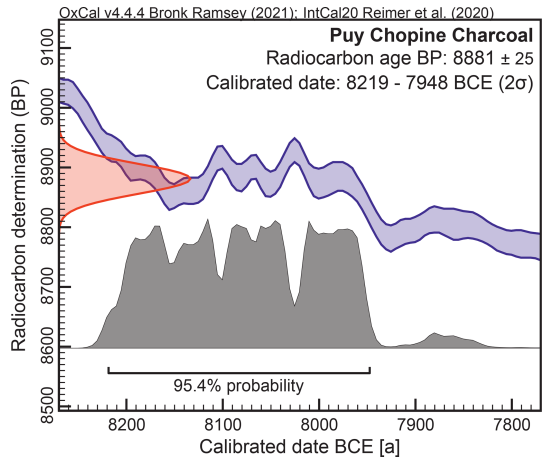

Figure 4. Example of a radiocarbon age calibration for a charcoal sample from Puy Chopine in the Chaîne des Puys volcanic field, France (McCreary, 2020). The probability distribution of the uncalibrated radiocarbon age is plotted on the y axis in red. This distribution is mapped onto the IntCal20 calibration curve (Reimer et al., 2020) in blue to determine the probability distribution of the calibrated age range in grey. The bar below the grey distribution represents the 95.4 % (2σ) confidence interval of the calibrated date. This example shows the effect of a small plateau in the calibration curve on the precision of the calibrated age.

and oceanic ^{14}C concentrations (Marine20; Heaton et al., 2020). While calibrated radiocarbon ages might be associated with an uncertainty of less than 2 %, there are several "age plateaus" present in the calibration curve which cause much higher uncertainties (see Guilderson et al., 2005). Such a plateau, known as the Hallstatt plateau, covers the Golden Age of Greece (5th century BCE), for which calibrated radiocarbon ages may have an uncertainty of several hundred years (i.e. > 10 %) (Hamilton et al., 2015; Jacobsson et al., 2018; Reimer et al., 2020).

Radiocarbon ages can also differ from the real age if the sample material was affected by reservoir effects, i.e. the initial $^{14}C / ^{12}C$ ratio incorporated by the material did not represent that of the atmosphere. This occurs particularly in ocean water, where CO_2 depleted in ^{14}C is taken up by organisms (Craig, 1957; Gordon and Harkness, 1992; Mangerud, 1972). It is important to note that the marine reservoir effect is highly dependent on local conditions and may change with time (e.g. Alves et al., 2018; McNichol and Lindauer, 2022). To correct for this effect, the local parameter ΔR that represents the offset compared to the real age of a sample must be determined (Stuiver et al., 1986b; Stuiver and Polach, 1977). This correction typically accounts for several hundred years. There is also a known freshwater reservoir effect that results in radiocarbon age overestimations for samples that developed in lakes and rivers influenced by so-called "hardwater" (Deevey et al., 1954; MacDonald et al., 1987; Philippsen, 2013). This hardwater is rich in dissolved carbonates from calcium carbonate rocks in the surrounding geology that are either depleted in ^{14}C or completely lacking ^{14}C (in this case known as "dead carbon") due to their older age. Philippsen (2013) reported radiocarbon age differences as high as 2 ka among modern samples from the same river due to this freshwater reservoir effect. Volcanic and hydrothermal settings associated with degassing of magmatic CO_2, which completely lacks ^{14}C, also present reservoir effects that result in age overestimation (Calderoni and Turi, 1998).

All the above highlights that caution is required when using published radiocarbon dating results. In the early years of radiocarbon dating (up to the 1980s), most of the previously mentioned problems were poorly understood or simply unknown. This applies particularly to contamination and reservoir effects. While data published before 1980 should be approached with caution, they can potentially be used when details regarding preparation and measurement procedures are provided (e.g. Millard, 2014). This includes the uncalibrated radiocarbon ages (in ^{14}C yr BP) to which the most up-to-date calibration can be applied. Furthermore, it is mandatory that the nature of the dated material (wood, shell, bone, peat, etc.) is noted and its stratigraphic context is clearly documented.

4.2 Radiocarbon dating in volcanic contexts

In the volcanic context, it must be noted that products of the eruption itself are not dated by radiocarbon. Instead, organisms killed or covered by the event are dated as a proxy. Hence, detailed documentation of the stratigraphic context is needed to establish whether the sample material was recovered directly from volcanic products or from strata below or above the volcanic material. In the most ideal case, the death of the organic material is coincident to the eruption itself. This sample material would thus be sampled directly from a volcanic stratum with evidence that it had been burnt during an eruption. Examples of this kind of material are remains of trees burnt by lava flows and charcoal samples from pyroclastic flow deposits (Lockwood and Lipman, 1980). These are both good sample materials for radiocarbon dating, particularly when younger than 25 ka (Higham et al., 2009).

In situations where volcanic material is covering older deposits or is covered by younger deposits, the results would pre- or post-date the eruption. Ideally, the volcanic deposit will be closely bracketed by organic material on both sides that can be dated to obtain a narrow range between the maximum and minimum age. The potential sample materials for this type of dating are palaeosols beneath lava flows, and peat or gyttja strata observed in sediment, often found far from the source volcano (Juvigné et al., 1996). It should be noted that these are not ideal sample materials for radiocarbon dating due to their high potential for contamination and often low carbon content (Evin, 1992; Juvigné et al., 1996; Shore et al., 1995). In cases where these materials have been used for radiocarbon dating, supplementary palynological data can help to confirm the accuracy of the resulting ages.

In addition to these sample material considerations, in volcanic contexts a special type of reservoir effect has been associated with the degassing of magmatic CO_2 (Calderoni and Turi, 1998). This ^{14}C-free CO_2 can be absorbed into the sample material, thus producing an age overestimate. This magmatic CO_2 affects soil humic acid fractions and is able to dilute the uptake of atmospheric ^{14}C by leaves in these settings. This reservoir effect is highly sensitive to spatial variations, as exemplified by a 5 ka range for radiocarbon ages measured from modern tree leaves sampled from the Solfatara crater in the Campi Flegrei, Italy (Calderoni and Turi, 1998). Samples that have been exposed to magmatic degassing over time should thus be closely investigated for contamination. For the First Millennium Taupo eruption in New Zealand, Holdaway et al. (2018) showed that radiocarbon ages could be overestimated by up to 200 a, in this case more than 10 % (Hogg et al., 2019; Holdaway et al., 2019).

4.3 Examples of radiocarbon dating applied to volcanism

Radiocarbon dating has established reliable eruption chronologies for many volcanoes and volcanic fields around the globe. One example of this is Vulcano, the southernmost Aeolian Island (Italy), for which a detailed eruption history between 900 and 1600 CE is available. Malaguti et al. (2022) present a revised chronology for eruptive activity in this period based on radiocarbon dating in combination with stratigraphic and palaeomagnetic analyses. They excavated twenty 2–3 m deep trenches around the La Fossa and Vulcanello cones, which allowed them to collect five different charcoal samples for radiometric dating. These samples were measured by AMS, after pre-treatments with HCl to remove absorbed carbonates and a special acid-base-acid pretreatment for charcoal as described by Brock et al. (2010). After calibration using the IntCal20 calibration curve, the integration of these ages with tephrostratigraphic and palaeomagnetic data helped to reveal that the La Fossa caldera experienced at least 19 eruptions from 900 to 1550 CE, which reflects one event per 35 a. This rate is much higher than the previously expected average reoccurrence rate of 130 a.

Another example of radiocarbon dating of volcanism is the work done on Mt. Fuji by Obrochta et al. (2018), which highlights the importance of precise chronologies for hazard assessments. Mt. Fuji, adjacent to the Tokyo metropolitan area, Japan, has been hazard mapped based on a chronology constrained by ages that are out of stratigraphic or geographic order. To overcome this, Obrochta et al. (2018) constructed a Holocene eruption history for Mt. Fuji through radiocarbon dating of lacustrine sediments in combination with tephrochronology. This study reported a refined 8 ka eruption history revealing previously unknown eruptions. They performed high-density radiocarbon dating on terrestrial macrofossils and bulk organic material from sediment cores sampled from Lake Motosu at the northwestern base of Mt. Fuji. The samples were measured with AMS and calibrated with the IntCal13 calibration curve. The impact of older carbon in the lake water on the bulk organic matter samples, one of the previously described reservoir effects, was mitigated by dating the bulk organic matter sampled at two depths corresponding to tephra of known age. These ages were used to reverse calibrate the other ages based on a methodology described in Lougheed et al. (2017). This use of lacustrine sediments allowed for closely spaced events to be clearly differentiated in the eruption chronology.

The final example of radiocarbon dating presented here is the eruption of the Santorini volcanic system in the Aegean Islands, Greece. Known as Thera in ancient Greek, the eruption chronology of this volcano is probably the most prominent controversy regarding the dating of a volcanic event. Since Marinatos (1939), this eruption has been suggested as a cause for the decline of the Minoan advanced civilisation during the Late Bronze Age, an important issue for understanding the history of the Mediterranean. Traditionally, the timing of the large eruption of Thera was placed ca. 1520 BCE, based on historical ages available from the Minoan and Egyptian cultures (e.g. Bietak, 2003; Ritner and Moeller, 2014). However, since the 1970s this age has been repeatedly challenged by radiocarbon dating, which has produced ages some 100 to 150 a older (Bronk Ramsey et al., 2004). Based on more than 100 radiocarbon samples, mostly short-lived organic material like seeds and grains, and complex statistical analyses, Bronk Ramsey et al. (2004) derived a likely age of 1663 to 1599 BCE for the Thera eruption. This age estimate was confirmed and narrowed down by the dating of an olive branch from Thera itself to 1627 to 1600 BCE (Friedrich et al., 2006). Since then, dozens of articles attempting to explain the offset and/or supporting the older radiocarbon-dated or archaeological-derived eruption age have been published (e.g. Bietak, 2014; Bruins and Plicht, 2025; Manning, 2022). The impact of magmatic CO_2 degassing on these radiocarbon ages has been considered as one possibility for the age discrepancies (Pearson et al., 2018). In recent years, potential anomalies in the calibration curve for the period of interest have been investigated to explain the apparent offset. However, this has provided support for both the younger and older age interpretations of the eruption (Friedrich et al., 2020; Manning et al., 2020; Pearson et al., 2018, 2023; Erdil et al., 2026). This situation is a good example of the complications to age interpretation that result from imperfect calibration curves.

5 Uranium-series-related dating

The principles of uranium (U) and thorium (Th) decay series dating started to be understood at the end of the 19th century when Henri Becquerel, Marie Curie, and Pierre Curie discovered radioactivity and the radioactive properties of U and Th (Becquerel, 1896; Curie, 1903). Two isotopes of U

(^{238}U and ^{235}U) and one isotope of Th (^{232}Th) are parent isotopes of three complicated decay chains that end with stable child isotopes of lead (^{206}Pb, ^{207}Pb, and ^{208}Pb, respectively; Fig. 5). These decay chains are composed of a variety of intermediary radionuclides produced through alpha or beta particle emission. These intermediate radioisotopes have half-lives ranging from a fraction of a microsecond to 245 ka, all of which are much shorter than the half-lives of the three parent U and Th isotopes. The relative abundance of these intermediate child isotopes is controlled by the decay rate of the parent isotope (i.e. the production rate of the child isotope) and the decay rate of the child isotope itself. In radioisotope systems where the half-life of the parent isotope is much longer than that of the child isotope, a steady state is achieved where the decay rate of the child equals its production rate. This steady state, known as secular equilibrium, is established after roughly six child isotope half-lives (Bourdon and Sims, 2003). After about 1 Ma, all intermediate isotopic systems of the U–Th decay chains will have reached a state of secular equilibrium, assuming the system remained closed. This state is known as complete secular equilibrium and allows the intermediate isotopes to be ignored. Radiometric dating using the U–Th parent and stable child Pb isotopes on samples with complete secular equilibrium is known as U–Th–Pb dating. U–Th–Pb dating is used to date some of the oldest rocks on Earth, due to the very long half-lives of the initial U–Th parent isotopes. The lower limit of these dating methods is determined by the time needed to establish complete secular equilibrium ($\sim$ 1 Ma).

If there is secular disequilibrium somewhere in the U–Th decay chains, this disequilibrium can be analysed to obtain geochronological information on timescales from a few hundred years up to 600–700 ka, depending on the intermediate isotopes used and if the system remained closed (Cheng et al., 2013). Disequilibrium can occur in any of the intermediary isotopic systems due to a variety of phenomena. Geochemical differences between parent and child isotopes result in their fractionation during geological processes such as crystallisation, partial melting, and weathering. For example, U is water soluble in its U^{+6} oxidation state, while Th is completely insoluble. This means that any carbonate rocks that precipitate from water will be in secular disequilibrium, because they will lack the intermediate child isotope ^{230}Th in the ^{238}U decay chain. In this case, the degree of disequilibrium between ^{234}U ($t_{1/2} = 246$ ka) and ^{230}Th ($t_{1/2} = 75$ ka) can be used to determine the amount of time elapsed since precipitation of the carbonate. The intermediate isotopes of most interest for disequilibrium dating are ^{234}U, ^{230}Th, and ^{226}Ra in the ^{238}U decay chain, and ^{231}Pa in the ^{235}U decay chain (Bourdon et al., 2018).

U–Th–Pb dating and U–Th series disequilibrium dating are not the only ways to obtain chronological information from the nuclear physics of U and Th. Geochronological methods using by-products of these decay chains have also been developed. One of these methods is "fission track dating". In addition to alpha decay to ^{234}Th, ^{238}U also decays at a known and constant rate through spontaneous fission into two lighter nuclei. These "child" nuclei damage the crystalline lattice they pass through after fission, leaving behind what is known as a fission track that can be made visible by etching a polished surface of a mineral. In U-rich minerals such as zircon, apatite, and glass, the density of fission tracks and the U content of the mineral can be measured to determine the amount of time passed since the crystal cooled below a known closure temperature, above which the tracks are annealed. As was the case for Ar, this closure temperature is also mineral dependent and should be thought of as a range instead of a specific temperature. This range is 320 to 210 °C for zircons (Yamada et al., 1995) and 125 to 60 °C for apatite (Gleadow and Duddy, 1981). The comparable range for glass varies greatly by composition and water content, with closure temperatures nearing the ambient range in some cases (Lakatos and Miller, 1972). As these fission tracks are thermally sensitive, they can also be used to decipher the thermal history of a rock. While fission tracks can be detected on a practical level after 100 ka, their use for dating is most reliable and widely used in the range from one to hundreds of Ma (Fleischer et al., 1964).

Another by-product of the U–Th decay series that can be used for dating is radiogenic helium (He) produced by alpha decay. Alpha particles (positively charged particles consisting of two neutrons and two protons) released during alpha decay are essentially nuclei of ^{4}He atoms. As soon as an alpha particle is stopped, it captures two electrons, thus becoming an atom of radiogenic He gas trapped in a mineral. The potential for this radiogenic He to escape from the crystal is controlled by the atomic-recoil distance, crystal morphology, and thermally dependent diffusion processes. Similarly to the ^{40}K / ^{40}Ar and ^{40}Ar / ^{39}Ar dating method, this accumulation of He in a crystal can be used to determine the time elapsed since the mineral cooled below a closure temperature of 290 to 210 °C for zircons in volcanic rocks (Danišík et al., 2017). This method is known as (U–Th) / He dating. He is unique as a child product of the U–Th series because it is produced by several parallel decay steps. For samples in complete secular equilibrium, there are relatively simple equations that can be used to obtain ages (Wolf et al., 1998). In samples where there is potential disequilibrium in the system, analysis of the disequilibrium is needed to properly model the He production rate and therefore obtain a reliable age (Farley et al., 2002). This method has found a variety of applications, most commonly on zircons, in the field of thermochronology due to the thermal sensitivity of He diffusion processes (Farley, 2002; Reiners et al., 2004).

5.1 Procedures, problems, and applications

The dating of lavas through ^{230}Th–^{238}U disequilibria was developed in the late 1960s with the internal isochron method (Allegre, 1968; Kigoshi, 1967). Due to differences

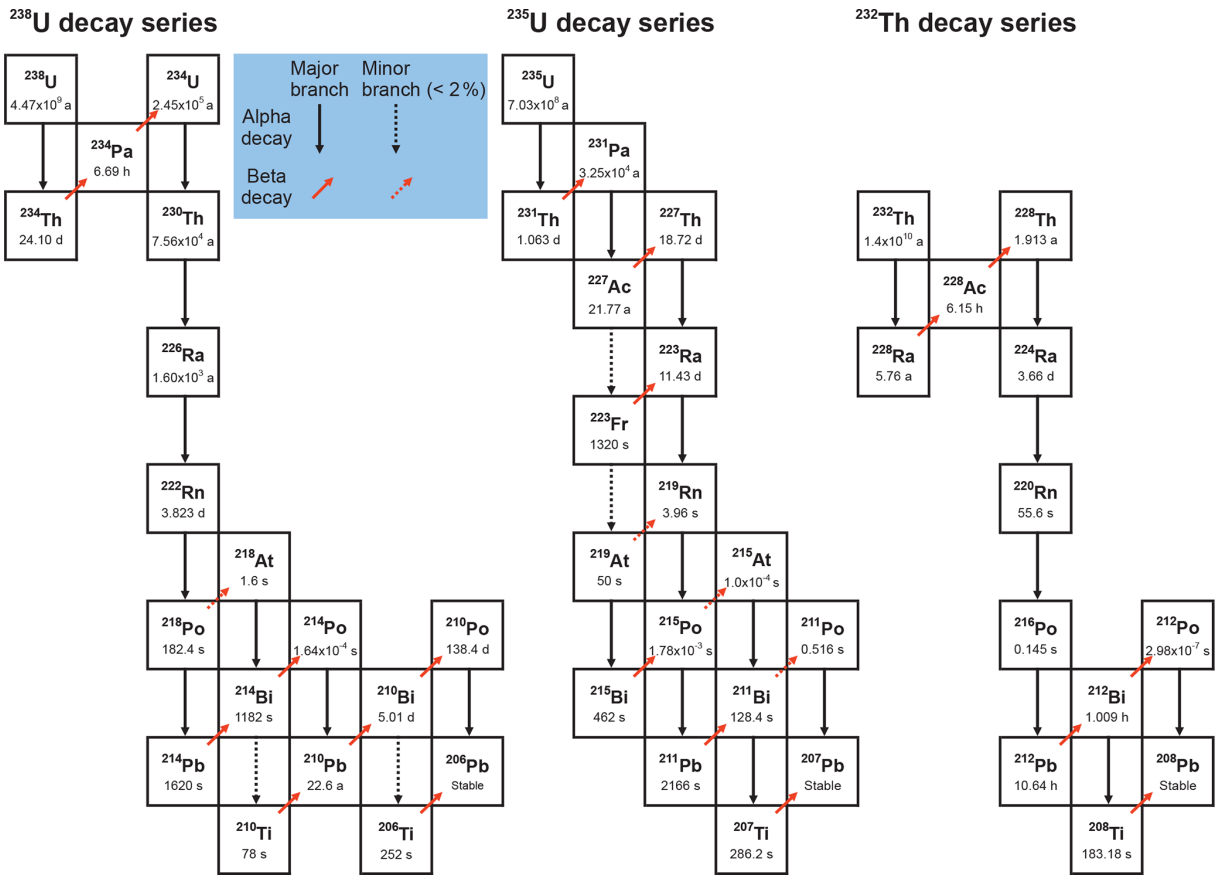

Figure 5. Decay chains of the ^{238}U, ^{235}U, and ^{232}Th isotopes. The half-lives of the isotopes are printed below each isotope. Black arrows indicate alpha decay, while red arrows indicate beta decay. The dashed arrows represent minor decay branches that account for less than 2 % of the isotope's total decay. All half-life values are taken from Haynes (2016).

in U and Th partition coefficients, minerals in a volcanic rock will crystalise with different (^{238}U / ^{232}Th) ratios but will have the same initial (^{230}Th / ^{232}Th) ratios. If the ratios for individual mineral phases are plotted together in a (^{230}Th / ^{232}Th) vs (^{238}U / ^{232}Th) diagram, they should form a line, known as an internal isochron (Fig. 6). The slope of this isochron (m) can be used to obtain a crystallisation age for the sample through Eq. (2):

$$t = \frac{\ln(1-m)}{\lambda_{230}}, \tag{2}$$

where λ_{230} is the decay constant of ^{230}Th. At $t = 0$, the points would form a horizontal line with a y intercept representing the (^{230}Th / ^{232}Th) for the system as a whole. At $t = \infty$, the slope will be equivalent to the "equiline" representing secular equilibrium.

The ideal sample material for U-series disequilibrium dating is lava that shows no signs of weathering or secondary alteration (Danišík et al., 2017). To create an isochron, it is necessary to measure at least two mineral phases (e.g. quartz, glass, olivine, or amphibole) from the same rock but ideally more (Taddeucci et al., 1967). The range of the

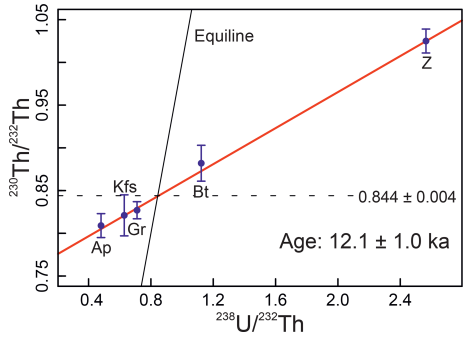

Figure 6. ^{230}Th / ^{238}U isochron diagram constructed from five mineral phases (Ap = apatite, Kfs = K-feldspar, Gr = groundmass, Bt = biotite, Z = zircon). The slope of the red isochron is used to calculate the crystallisation age of 12.1 ± 1.0 ka. The dashed line represents the initial ^{230}Th / ^{232}Th ratio for all phases at the time of crystallisation, which corresponds to the whole-rock ^{230}Th / ^{232}Th ratio. Plot reproduced from data published in Condomines (1997).

^{238}U / ^{232}Th ratio in a mineral impacts the precision of its measurement. For this reason, zircon, an accessory mineral

in juvenile volcanic rocks with a high ^{238}U / ^{232}Th ratio, is valuable for disequilibrium dating (Cerrai, 1965; Fukuoka and Kigoshi, 1974). In the early days, ^{230}Th–^{238}U disequilibrium measurements required relatively large amounts of sample material, 1 to 3 g of each mineral, prepared as mechanical mineral separates or isotope dilutions (Taddeucci et al., 1967). U and Th isotope abundances were then directly measured through mass spectrometry, or the ^{230}Th / ^{232}Th and ^{238}U / ^{232}Th activity ratios were measured by alpha spectrometry (Condomines, 1997). Technological advancements in the field of mass spectrometry, for example, the development of thermal ionisation mass spectrometry (TIMS), secondary ion mass spectrometry (SIMS), laser ablation inductively coupled plasma mass spectrometry (LA-ICP-MS) and the sensitive high-resolution ion microprobe (SHRIMP) have greatly improved the measurement of isotope ratios for analysing disequilibrium and have even facilitated nearly non-destructive measurements on individual crystals.

The zircon double dating (ZDD) technique was developed to better understand differences in crystallisation and eruption ages for Quaternary volcanism (Danišík et al., 2012, 2017; Schmitt et al., 2006, 2011). This technique dates accessory zircons in lava with both ^{230}Th / ^{238}U disequilibrium and (U–Th) / He dating to provide eruption ages in the range from 2 to 1000 ka (Danišík et al., 2017). Since He only accumulates in rapidly cooled volcanic zircons after they cool below 210–290 °C, the (U–Th) / He age is a good approximation of the eruption age (Danišík et al., 2017). However, because disequilibrium in the U–Th decay series has an important impact on He production rates, ages are often underestimated by the (U–Th) / He method (Danišík et al., 2017). ^{230}Th / ^{238}U disequilibrium dating contributes to ZDD by quantifying the amount of disequilibrium in the system, thus facilitating the necessary corrections to the (U–Th) / He age. ZDD has the advantage that both dating methods can be applied to the same zircon crystals. First, nearly non-destructive microprobe methods like SIMS, SHRIMP, or LA-ICPMS are used for U–Th disequilibrium dating. Then, a morphological and U–Th zonation characterisation of the zircon crystal is performed to allow for a later atomic-recoil correction to the (U–Th) / He age. Finally, whole-grain bulk analysis of U, Th, and He is performed on the zircon. This entails a degassing of the crystal at ∼ 1250 °C under ultra-high vacuum to extract He that is measured through noble gas mass spectrometry. This measurement step can be a challenge if the levels of He in the zircons are near the detection limit, creating a lower limit to ZDD (Danišík et al., 2017). Despite this, ZDD ages as young as 2 to 2.5 ka have been obtained for zircons from volcanic products (Marsden et al., 2021; Schmitt et al., 2013). The remaining zircon is then completely dissolved in acid to measure U and Th through isotope dilution and ICPMS. The bulk abundances of He, U, and Th are then used to calculate a "raw" (U–Th) / He age. This raw age is corrected for both atomic recoil loss of He and for disequilibrium effects. The He atomic-recoil correction can have a significant impact, with corrected ages often being up to 30 % higher than the raw age (Farley et al., 1996). The correction for U–Th disequilibrium can be performed through Monte-Carlo simulation with the atomic-recoil-corrected (U–Th) / He age, the U–Th disequilibrium crystallisation age, and two parameters that describe the zircon-melt fractionation of ^{230}Th and ^{231}Pa in relation to U as inputs. While ZDD has only been explored for a few decades, it is a promising method for future dating campaigns of volcanic landforms.

5.2 U-series dating in volcanic contexts

The preferred isotopes for studying magmatic processes are the child products of the ^{238}U and ^{235}U decay chains. These isotopes help to elucidate information about crustal residence time and the timescale of melt transportation (Condomines et al., 2003). The main processes that cause secular disequilibrium in magmatic systems are partial melting, magma differentiation, and fractional crystallisation. When mantle rock, assumed to be in secular equilibrium, undergoes partial melting, fractionation occurs between the parent and child isotopes. This is because the isotopes have different partition coefficients between the mineral phase and the melt. For example, compared to ^{234}U, ^{230}Th has a greater affinity to transition from the mineral phase of the rock into the melt. Thus, lava formed from the melt will have a glassy matrix in secular disequilibrium due to a surplus of ^{230}Th, while the phenocrysts will be in various degrees of disequilibrium due to a lack of ^{230}Th. Furthermore, phenomena such as hydrothermal alteration (Villemant et al., 1996) and fluid addition (Turner et al., 2003) also result in secular disequilibrium. Following these processes, the disequilibrium between isotopes of the same decay chain can be quantified, and the type of perturbation the system received to produce the observed disequilibrium can be inferred.

It is important to remember that the isochron method of ^{230}Th / ^{238}U disequilibrium dating only provides crystallisation ages. While crystallisation ages can correspond with the eruption age, there are published ^{230}Th / ^{238}U disequilibrium crystallisation ages much older than eruption age estimates, indicating an extended residence time in the magma chamber before eruption (see Bourdon et al., 1994; Volpe and Hammond, 1991). For this reason, it is recommended that ^{230}Th / ^{238}U disequilibrium ages for volcanic samples be interpreted as maximum ages for eruptions. For a more detailed discussion of the ways U-series dating of accessory minerals can be used to quantify a variety of volcanic processes, readers are directed to Schmitt (2011).

5.3 Examples of U-series dating applied to volcanism

U-series dating methods have been applied to volcanism from the early development of U–Th–Pb dating and U–Th disequilibrium dating to the development of the ZDD ap-

proach in the early 21st century – to varying degrees of success. One representative example of disequilibrium dating is the use of ^{230}Th / ^{238}U disequilibrium in accessory minerals to date trachytic lava from the Puy de Dôme, France, by Condomines (1997). The Puy de Dôme, a trachytic dome volcano, is the highest summit in the Chaîne des Puys volcanic field and has a complex formation history. Before Condomines (1997), Puy de Dôme products had been dated through radiocarbon and luminescence methods (Faïn et al., 1988, 1991; Juvigné and Gewelt, 1987). In his study, Condomines (1997) sampled trachytic lava from the first phase of dome construction, which contained phenocrysts of oligoclase, sanidine, biotite, and clinopyroxene, as well as inclusions of apatite and zircon in the groundmass. The lava was separated into the following fractions for dating: groundmass, sanidine, biotite, apatite, zircons, and a whole-rock sample containing all the previously mentioned fractions. After chemical treatments to digest the fractions into solutions, the U and Th abundances were measured with mass spectrometry and the ^{230}Th / ^{232}Th and the ^{234}U / ^{238}U activity ratios were measured with high-resolution alpha spectrometry. The ^{234}U / ^{238}U activity ratios of all fractions indicated equilibrium levels, which allowed direct analysis of the disequilibrium between ^{238}U and ^{230}Th. An isochron diagram plotted from these five fractions presents a well-defined isochron (Fig. 6). The slope of this isochron gave a crystallisation age of 12.1 ± 1.0 ka (1σ) for the lava, and the intercept with the equiline indicates an initial ^{230}Th / ^{232}Th ratio of 0.844 ± 0.004. While this age corresponds to the crystallisation of the various phenocrysts, it agrees with previous luminescence and radiocarbon ages for Puy de Dôme deposits (TL: 10.8 ± 2, 9.8 ± 1, and 9.7 ± 1 ka; Faïn et al., 1988, 1991; ^{14}C: 9.79 ± 0.275 BP or 11 819–10 683 cal BP; Juvigné and Gewelt, 1987), despite being slightly younger estimates. Assuming the luminescence and radiocarbon ages are reliable, these results support an eruption age from 12 to 11 ka and a short interval of not more than a few centuries between crystallisation and eruption.

The disadvantage of U–Th disequilibrium dating is that it only provides crystallisation ages, which in some cases could be quite different from eruption ages. The ZDD approach overcomes this issue by using the results of U–Th disequilibrium analysis to improve the results of (U–Th) / He dating. An early application of this approach was performed by Schmitt et al. (2006) to date the Las Tres Vírgenes volcano in Baja California, Mexico, which was thought to be historically active due to present-day hydrothermal activity. They sampled pumice from the La Vírgen tephra that was carefully selected, cleaned, and crushed to avoid unwanted material. In addition to a whole-rock fraction of the pumice, individual zircon grains were isolated. Non-destructive SIMS was performed on individual grains with an ion microprobe capable of focusing on a $\sim 35 \times 30$ µm spot. The La Vírgen tephra whole-rock U and Th concentration was analysed with TIMS, and the ^{230}Th / ^{232}Th ratio was measured with SIMS. The whole-rock results were in secular equilibrium and were therefore also analysed for U–Th–Pb dating. In contrast, many of the zircons were not in equilibrium and could be used to construct an isochron diagram. The slope of the resulting isochron was calculated through two methods that yielded similar results within uncertainties: U–Th disequilibrium ages of 121 ± 12 or 118 ± 15 ka. These ages relate to when crystallisation of the zircons stopped. To complete the (U–Th) / He dating, the U, Th, and He abundance of eight zircons was measured through isotope dilution and noble gas mass spectrometry. The resulting average (U–Th) / He age for the eight zircons was 29 ± 2 ka, but this is merely a minimum age estimate as it does not account for disequilibrium of ^{230}Th in the system due to fractionation between Th and U during zircon crystallisation. To resolve this, the SIMS and TIMS U / Th values for the zircons and whole-rock samples were used to calculate mineral-melt partitioning coefficients and the residence time of the zircons in the magma before eruption. These coefficients, along with the U–Th disequilibrium and (U–Th) / He ages and uncertainties, were then used to correct for the disequilibrium and the residence time of the zircons in the magma. In this case, the average of the corrected (U–Th) / He eruption ages for the zircons was 36 ± 6 ka. This age contrasts with the previously published radiocarbon age of 6516 ± 75 BP for a single piece of carbonised wood from the middle of the tephra (Capra et al., 1998) and a reference in an 18th century map to a 1746 eruption (Ives, 1962) However, the ZDD age is supported by a ^{3}He cosmogenic nuclide exposure age of $> 26 \pm 4$ ka for a basaltic lava flow overlying the La Vírgen tephra (Hausback and Abrams, 1996). As the radiocarbon age is based on only one sample, there are several possible explanations why it is so young, such as sample alteration. It is also possible that the sample is from a wildfire and only became entrained in the tephra after a reworking event like a landslide. The historical records also have the potential to be misinterpretations of a steam release from the hydrothermal activity, debris from a landslide, or even smoke from a wildfire. For these reasons, and the support of the ^{3}He cosmogenic nuclide exposure age, this ZDD age is considered reliable.

6 Cosmogenic nuclide exposure dating

Cosmogenic nuclide exposure dating is a geochronological technique used to determine the exposure age of rocks and sediments on Earth's surface. This technique is based on the production and accumulation of isotopes called terrestrial cosmogenic nuclides (TCNs) in minerals and sediments showered by cosmic-ray-derived particles known as "secondary cosmic ray particles" (see reviews in Lal, 1991; Gosse and Phillips, 2001; Ivy-Ochs and Kober, 2008; Dunai, 2010). When high-energy cosmic rays interact with atoms in the atmosphere, both TCNs and secondary ray particles are produced. These secondary ray particles, mostly neutrons and

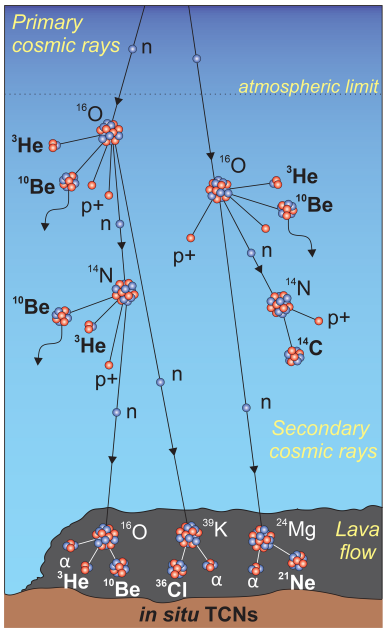

Figure 7. Schematic illustrating the production of TCNs (^{3}He, ^{10}Be, ^{21}Ne, ^{36}Cl) in the atmosphere and in lava by cosmic rays.

muons, cascade down to the surface of the Earth, producing more TCNs and secondary ray particles with each collision (Fig. 7). When this cascade of secondary ray particles reaches the Earth's surface, they produce TCNs inside exposed minerals through interactions with "target" elements present in the mineral. The resulting TCNs take the place of the target element in the crystalline lattice. Through measuring the concentration of TCNs accumulated over time in a rock sample and estimating the location-specific production rate of TCNs, it is possible to estimate the surface exposure time of the rock.

6.1 Procedures, problems, and applications

There are several TCNs used for cosmogenic nuclide exposure dating. These TCNs can be either long-lived radionuclides (e.g. ^{10}Be, ^{14}C, ^{26}Al, ^{36}Cl) or noble gases (e.g. ^{3}He, ^{21}Ne). An overview of the characteristics of the main TCNs used for cosmogenic nuclide dating is reported in Table 1. The main types of interaction that produce these TCNs are spallation by neutrons, muons, and neutron capture. For example, secondary ray particles that interact with a quartz crystal can produce beryllium-10 (^{10}Be) through spallation of oxygen atoms in the quartz (Fig. 7). TCN concentrations are measured by mass spectrometry (AMS, for radionuclides; noble gas spectrometry for noble gases).

In addition to the concentration of TCNs, the rate at which the TCN is produced (the so-called production rate) and the rate at which unstable TCNs decay (half-lives of radionuclides) must also be known. Production rates vary depending on the nuclide considered and on the sample location. Rates are higher at high altitudes and high latitudes due to reduced atmospheric shielding and at high latitudes due to an increased flux of cosmic rays resulting from the geometry of the Earth's magnetic field. Scaling schemes have been developed to model the production rate at a sampling site based on the production rate derived at the closest neighbouring calibration site. These scaling schemes have been refined in recent years following an improved understanding of TCN production pathways (Balco et al., 2009; Lifton et al., 2014; Martin et al., 2017). This refinement, however, has led to potential discrepancies between original and rescaled ages.

TCN production rates also decrease with depth into a rock or sediment, since the flux of secondary cosmic ray particles (neutrons in particular, muons to a lesser extent) is attenuated with depth. Consequently, erosion leads to a decrease in the TCN concentration of the sampled surface, potentially resulting in age underestimation. Rock surfaces unaffected by erosion should therefore be targeted for dating. When this is not possible, a correction for erosion should be included if independent erosion estimates are available.

Two additional issues regarding cosmogenic nuclide dating are (a) inheritance of nuclides from previous exposure periods (see Ivy-Ochs et al., 2009) and (b) the interruption of surface exposure by periods of surface shielding (e.g. Delunel et al., 2014). Such complex exposure histories can lead to age over- and underestimation, respectively. These issues can potentially be resolved by studying combinations of radioactive TCNs with different half-lives (^{10}Be–^{26}Al, e.g. Fabel et al., 2002; ^{14}C–^{10}Be, e.g. Hippe, 2017; ^{10}Be–^{21}Ne, e.g. Balco et al., 2014). Paired radionuclides will be in disequilibrium after a period of surface shielding due to their differential decay rates. This disequilibrium can give information about nuclide inheritance or interrupted surface exposure (Hippe, 2017).

The upper and lower age limits for cosmogenic nuclide dating depend on both methodological and geological factors. The lower limits are set by analytical sensitivity (i.e. the minimum TCN concentration sufficient for robust quantification). Exposure ages of a few hundred years can be determined when working with ^{3}He, the TCN with the highest production rate and a low detection limit (Table 1; Blard, 2021). Upper age limits are constrained by the radionuclide decay rate and by the erosion rate of the investigated rock surface. The concentration of a TCN in a rock surface increases with exposure until saturation. For stable TCNs, saturation occurs when there are no more atoms of the target element to produce new TCNs. In the case of radioactive TCNs, saturation occurs when an equilibrium in the production and decay of the TCN is reached. The exposure time needed to reach this saturation equilibrium level corresponds to ca. three to four half-lives of the considered radionuclide. This consequently sets the maximum exposure age that can be determined for the corresponding TCN. Depending on the TCN considered, upper age limits vary between ca. 50 ka for ^{14}C and several millions of years for ^{3}He and ^{21}Ne. The oldest

Table 1. Details about the main cosmogenic nuclides used for exposure dating. Information from Dunai (2010) and von Blanckenburg and Willenbring (2014).

TCN	Half-life	Main target elements	Main target mineral	Interaction + contribution (%)	Production rate at SLHL[a] (atm g^{-1} a^{-1})
^{3}He	Stable	All major elements + Li	Olivine, pyroxene, He-retentive minerals	Spallation: 100 Li: thermal neutron capture	75 to 120
^{10}Be	1.4 Ma	O, Si	Quartz (rarely pyroxene and olivine)	Spallation: 96.4 Muon: 3.6	4 to 5
^{14}C	5720 a	O, Si	Quartz	Spallation: 82 Muon: 18	18 to 20
^{21}Ne	Stable	Mg, Al, Si	Quartz, pyroxene, olivine	Spallation: $>$ 96.4 Muon: $\leq$ 3.6	18 to 21
^{26}Al	0.7 Ma	Si	Quartz	Spallation: 95.4 Muon: 4.6	35
^{36}Cl	0.3 Ma	K, Ca, ^{35}Cl, (Fe, Ti)	Carbonates, feldspar, whole rock	K: spallation 95.4; muons 4.6 Ca: spallation 86.6; muons 13.4 Fe, Ti: spallation presumed 100 Low-energy neutron capture produces ^{36}Cl from Cl and K.	70 (Ca), 200 (K)[b]

[a] SLHL: production rate at sea level and high latitude. [b] ^{36}Cl production rate depends on concentration of Ca, K, and ^{35}Cl in minerals.

known exposure ages ($>$ 10 Ma) so far were obtained with ^{3}He (Balter-Kennedy et al., 2020).

6.2 Cosmogenic nuclide dating in volcanic contexts

The development of cosmogenic nuclide dating over the last decades has allowed the establishment of chronological constraints on many fields of Earth sciences, including volcanic systems (Bromley et al., 2019; Espanon et al., 2014; Fenton et al., 2004). Volcanic products are well suited for cosmogenic nuclide dating since their newly formed surfaces are not affected by nuclide inheritance. One difficulty lies in identifying the original post-eruptive surface. This can be recognised based on the presence of eruptive features (e.g. spatter, glassy texture of cooling rinds on flows, smooth surfaces of pahoehoe flows), the preservation of which indicates minimal erosion (Phillips, 2003). Another factor complicating cosmogenic nuclide dating of volcanics is the scarcity of production rate calibration sites for TCNs. When evaluating a cosmogenic nuclide age for a volcanic eruption, it is important that the calibration site for the production rate is geographically close enough to the eruption location to be meaningful. This highlights the need for new calibration sites to reduce potential inaccuracies in the spatial scaling of the production rate (Espanon et al., 2014; Blard, 2021).

Depending on the minerals and landforms targeted, different TCNs have been employed to constrain the chronology of volcanic eruptions. The TCNs ^{3}He and/or ^{21}Ne are used on olivine and pyroxene minerals in lava flows (e.g. Fenton et al., 2009; Gillen et al., 2010; Espanon et al., 2014; Doll et al., 2024). The high production rate of ^{3}He makes it ideal for dating young lava flows (i.e. Late Holocene to historical; Heineke et al., 2016; Doll et al., 2024). For both ^{3}He and ^{21}Ne, it is important to determine the contribution from non-cosmogenic sources of these isotopes (i.e. magmatic, radiogenic, and atmospheric) to the total concentration of ^{3}He and ^{21}Ne measured. Establishing these contributions enables a reduction of the uncertainty in the obtained exposure ages (Blard, 2021; Niedermann, 2002). Nonetheless, the combined application of ^{3}He and ^{21}Ne has shown great potential in the exposure dating of lava flows, since age intercomparison allows for the identification of outliers (Espanon et al., 2014; Fenton et al., 2009; Gillen et al., 2010).

Surface exposure of volcanic rocks lacking olivine and pyroxene (i.e. silicic lavas) can be dated through ^{36}Cl by sampling phenocrysts of Ca-rich feldspar (e.g. Bromley et al., 2019) or bulk rock samples (e.g. Alcalá-Reygosa et al., 2018; Phillips, 2003). ^{36}Cl is applicable to a wide range of minerals and rock types, as it is produced from several target elements (Table 1). Since the TCN production pathways vary depending on the concentration of the target elements, estimation of the ^{36}Cl production rate is complex (Schimmelpfennig et al., 2011). Furthermore, the low-energy neutron capture which produces ^{36}Cl from ^{35}Cl is difficult to estimate in bulk rock volcanic samples, which often contain high Cl concentrations in the glass matrix of the lava (Schimmelpfennig et al., 2009).

Lastly, ^{10}Be cosmogenic nuclide dating has also been employed to date volcanic activity through non-volcanic sample material. For example, ^{10}Be exposure dating has been

applied to quartz-bearing xenoliths (Heineke et al., 2016). Alternatively, silicic rocks exposed in the walls of volcanic landforms, such as maar craters, can be dated with ^{10}Be to provide a minimum age for the maar (Valentine et al., 2019). Using ^{10}Be in quartz presents the advantages of well-understood ^{10}Be production pathways, as well as well-established extraction and measurement procedures. Recent investigations have also shown progress in laboratory extraction procedures and production rate estimation of ^{10}Be in pyroxene (Balter-Kennedy et al., 2023). This development highlights the potential of using this nuclide–mineral pair to exposure date mafic rocks.

6.3 Examples of cosmogenic nuclide dating applied to volcanism

Examples of cosmogenic exposure dating applied to volcanism exist for a wide range of products and landforms. One of the most common examples is the surface exposure dating of lava flows. An example of this is the efforts by Espanon et al. (2014) to date two volcanoes in the Llancanelo and Payún Matrú volcanic fields, Mendoza, Argentina. These authors measured the accumulation of ^{3}He and ^{21}Ne in olivine separates from five samples of basalt: three from the surface of a lava flow and two from volcanic bombs believed to be undisturbed since eruption. The Mg content of the olivine was measured through X-ray fluorescence analysis, while He and Ne were measured through noble gas mass spectrometry. The combined application of measurement to ^{3}He and ^{21}Ne increased the confidence in the resulting ages as the two nuclides are stable, have similar characteristics, and can be measured from the same sample. The ages obtained for these samples confirmed eruptive activity as recent as 5 ka in the Payún Matrú volcanic field. However, their analysis was challenging due to the limited number of ^{21}Ne production rate calibration sites available, forcing Espanon et al. (2014) to use a production rate derived from a Northern Hemisphere calibration site. Very few production rate calibration sites are in the Southern Hemisphere, and scaling schemes often assume similar cosmic-ray fluxes in both hemispheres. This issue increases the uncertainty in the resulting ages because the Earth's geomagnetic field is not a perfect dipole (Cox, 1962; Laundal et al., 2017).

For a variety of reasons, the careful consideration of the volcanic material for dating is very important. An example of this is the dating of a Holocene eruption in the Kula volcanic field in western Türkiye. ^{3}He and ^{10}Be exposure dating were applied to olivine in basalt and to quartz-bearing xenoliths, respectively. In this case, the selection of sampling material was essential to rule out the presence of inherited ^{10}Be in the quartz. The xenoliths analysed by Heineke et al. (2016) were selected because they were located on top of the cone, had a rounded shape, and displayed a lithology distinct from the surrounding volcanic material. They also presented direct contact to lava. These are all indications that the xenoliths originated from the basement beneath the cone and were entrained by rising magma during the eruption, thereby excluding significant ^{10}Be inheritance.

A final example of the importance of sample selection is the ^{36}Cl nuclide dating of late Holocene lava flows from the Pico de Orizaba volcanic complex in the eastern portion of the Trans-Mexican Volcanic Belt (Alcalá-Reygosa et al., 2018). Samples of dacitic lava were collected from the top of two lava flows on the flanks of Pico de Orizaba, Mexico's highest stratovolcano. Blocks with protruding geometries were preferred due to a reduced risk of snow shielding. Due to the lack of adequate phenocrysts, ^{36}Cl produced in situ was measured for bulk rock samples of the lava. These samples contained high Cl concentrations (250–400 ppm), resulting in ∼ 60 %–70 % of the total ^{36}Cl production being derived from neutron capture on ^{35}Cl. Because the flux of low-energy neutrons responsible for this reaction is highly sensitive to environmental factors such as hydrogen content, snow cover, and surface geometry, the production rate was difficult to constrain. This resulted in relatively large uncertainties for the ages produced by these measurements (∼ 17 %–20 %). For this reason, it is generally preferable to measure ^{36}Cl on Ca- and/or K-rich minerals (e.g. feldspars or clinopyroxenes), rather than in bulk rock samples (Schimmelpfennig et al., 2009).

7 Luminescence dating

This group of methods uses mineral luminescence to determine the time elapsed since crystallisation, last exposure to sunlight (i.e. elapsed time since burial), or heating above ambient temperatures (for a sufficient duration dependent on temperature) for rocks, sediments, or archaeological samples. Luminescence is the emission of light from a mineral, mainly quartz or feldspar, upon stimulation by heat or light (see Aitken, 1985, 1998). This signal (i.e. the latent light emitted) gradually accumulates over time in mineral grains through trapped charge excited by environmental radiation from radioactive decay and cosmic rays. In contrast, the signal is rapidly reset to a zero level by heat or light. Randall and Wilkins (1945) proposed that the signal emitted is energy released as photons due to electrons returning to a ground state after being confined at defects in the crystalline lattice, known as "traps". A significantly simplified diagram of these phenomena can be found in the upper two panels of Fig. 8. Daniels et al. (1953) established the usefulness of this phenomenon for dating through identifying the relationship between luminescence signal intensity and the absorbed radiation dose. The intensity of a sample's natural luminescence signal can be converted into the amount of environmental radiation absorbed, known as the palaeodose or equivalent dose (D_e), through comparison to the signal intensity resulting from artificial irradiations of the sample. Finally, an age estimate can be calculated by dividing the D_e value (calculated

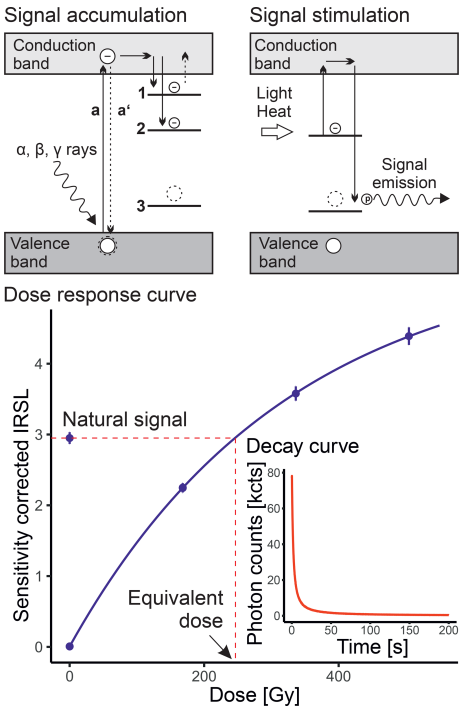

Figure 8. Upper two panels: Energy level diagrams illustrating the accumulation and release of a luminescence signal. Path (a) in the signal accumulation panel displays an electron becoming excited into the conduction band from the valence band by ionising radiation. Most excited electrons immediately dissipate this energy by recombining with a hole in the valence band, as indicated by path (a'). Alternatively, some excited electrons migrate through the conduction band to localised energy levels slightly below the conduction band known as electron traps (1 and 2). Trap 1 is shallower than trap 2, meaning it requires less energy to release the trapped electrons and is less thermally stable. When an excited electron is trapped, it leaves behind a hole in the valence band, which can migrate to hole traps that occupy an energy state slightly above the valence band (3). The signal stimulation panel displays how light or heat are able to stimulate the trapped electron back into the conduction band, from where it can recombine with a hole at the hole trap. In this process, a photon is released, which contributes to the luminescence signal. Lower panel: a representative dose response curve used to interpolate the D_e through a SAR protocol. The insert is an example of a luminescence decay curve.

in Gray; $1\,\mathrm{Gy} = 1\,\mathrm{J\,kg^{-1}}$) by the dose rate, i.e. the amount of radiation exposure per year at the sampling location. All luminescence dating methods share the same fundamental age equation – Eq. (3):

$$\text{Age [a]} = \frac{D_e\ [\mathrm{Gy}]}{\text{dose rate}\ [\mathrm{Gy\,a^{-1}}]}. \tag{3}$$

7.1 Procedures, problems, and applications

The measurement of two variables is required for luminescence dating: the D_e and the dose rate. The dose rate can be measured in situ when sampling with dosimeters or portable gamma-spectrometers. More commonly, samples are collected and measured to calculate the dose rate from the activities of radioactive elements in the target mineral (the internal dose rate) and in the surrounding material (the external dose rate). These measurements are usually made through high-resolution gamma spectrometry, neutron activation analysis, counting techniques (alpha, beta, gamma), or inductively coupled plasma mass spectrometry. For the external dose rate calculation, additional estimates of cosmic ray exposure and the average moisture content throughout time are also needed (Aitken, 1985). The dose rate calculation is often the more complicated component of a luminescence age and is the major source of systematic error (Mahan and DeWitt, 2019).

The D_e is obtained by comparing the sample's natural luminescence intensity to the intensity of the signal after irradiations of known amount. The most common approaches to determine the D_e in this context are extrapolation or interpolation. To extrapolate the D_e, varying amounts of laboratory radiation are added to the natural dose of multiple aliquots of the same sample (multiple aliquot additive dose (MAAD) protocols). Alternatively, the D_e can be interpolated by regenerating the luminescence signal in single aliquots at varying doses after first measuring the natural signal (single aliquot regenerative (SAR) dose protocols: Fig. 8; Murray and Wintle, 2000). Both approaches can be applied regardless of the luminescence stimulation method used.

There are several well-established methods to stimulate mineral luminescence for D_e determination. The first of these is thermoluminescence (TL), which uses gradual heating of the sample to 500 to 600 °C to stimulate the luminescence signal from thermally sensitive traps. In the 1980s, doubt was cast upon sediment dating using TL because of several TL age overestimates due to incomplete resetting of the signal (see Mahan and DeWitt, 2019). The two remaining methods of stimulation for luminescence, developed in the late 1980s, use illumination to release electrons from light-sensitive traps. For the measurement of quartz, visible light (wavelength ~ 470 nm) is used for stimulation, and the method is referred to as optically stimulated luminescence (OSL; Huntley et al., 1985). For feldspar, a similar method called infrared stimulated luminescence (IRSL) is applied, which utilises infrared light (wavelength ~ 850 nm) as stimulation (Hütt et al., 1988). For both OSL and IRSL, a preheat step is necessary to release electrons from unstable traps that were filled by laboratory irradiation (Wintle and Murray, 1998; Duller, 1994).

These measurement procedures are not without issues. The first issue to consider is a potential change in the sensitivity of the sample after repeated measurement cycles. The intense thermal treatments used in TL, the preheats used for OSL and IRSL, and even laboratory irradiation itself, all have the potential to change a sample's sensitivity to irradiation. This change in sensitivity could pose a significant obstacle to obtaining a meaningful D_e by comparing the natural lu-

minescence of a sample to regenerated luminescence signals with higher or lower sensitivity. Consequently, early TL work used MAAD approaches in which the aliquots are only irradiated and heated once in the measurement process. MAAD approaches, however, have greater random errors due to luminescence variability between individual aliquots. In response to these issues, Duller (1995) and Murray et al. (1997) developed SAR methods for feldspar IRSL and quartz OSL, respectively. These developments allow for the measurement and correction of sensitivity changes over repeated cycles of luminescence regeneration through the implementation of normalisation to a constant test dose response. Murray and Wintle (2000) incorporated these improvements into a single protocol that includes quality assurance tests and rejection criteria for individual aliquots if the sensitivity correction is not sufficient.

The second potential issue that needs to be considered is known as "partial resetting". This issue occurs when the natural luminescence signal of a sample is not completely and uniformly reset before burial (or another event that is dated). When undetected, this results in an age overestimation. Partial resetting is most common in fluvial or glacial settings where the transportation distance is short, and the water is potentially too turbid for all sediment grains to be completely reset by sunlight. Yet, it could occur in any situation where the cause of signal resetting is insufficient in either strength or duration. This issue can be mitigated by implementing luminescence protocols that measure the D_e of single grains of the sample (Olley et al., 1999). If there has been partial resetting, the D_e values will have an asymmetrical spread with a low population reflecting full resetting, and a higher gradually increasing population representing grains that were only partially reset. By evaluating the lower population of the D_e values, an age can be calculated by modelling the minimum age (Murray et al., 1995; Galbraith and Roberts, 2012).

The third issue facing luminescence dating, particularly of feldspars, is a phenomenon known as "anomalous fading". Wintle (1973, 1977) was the first to observe this phenomenon when she noticed a decrease in TL intensity after storage for short periods of time following irradiation. Spooner (1992) identified the same issue in feldspars measured through IRSL methods. This decrease in intensity is due to an athermal loss of signal over time from traps that should be stable on geological timescales. The proposed mechanism for this loss is electron quantum tunnelling (Visocekas, 1985; Visocekas et al., 1998; Guérin and Visocekas, 2015). The consequence of this fading is an age underestimation. Methods have been developed to quantify the rate of fading through laboratory storage tests, and corrections can be applied (Huntley and Lamothe, 2001; Auclair et al., 2003; Kars et al., 2008). However, some of the necessary assumptions underlying these corrections limit their use to samples younger than 50 ka in age with moderate to low fading rates (Huntley and Lian, 2006). Alternatively, the impact of anomalous fading can be reduced or eliminated by various preheating steps or by focusing on specific components of the luminescence signal which do not fade (Thomsen et al., 2008). The most successful examples of this approach are the post-IR IRSL (pIRIR) and multi-elevated-temperature post-IR IRSL (MET-pIRIR) dating protocols (Thomsen et al., 2008; Buylaert et al., 2009, 2012; Thiel et al., 2011; Li and Li, 2011, 2012). In these protocols, aliquots are first measured with a low temperature (50 °C) IRSL step to remove fading components, and then a stable signal of the same aliquot is measured with IRSL at higher temperatures (180, 225, or 290 °C). These methods, which have been applied similarly to single aliquots and single grains, have rejuvenated research into feldspar as a target material for luminescence dating.

Luminescence dating is predominately used to obtain burial ages for sediments of various kinds. Current SAR protocols allow the D_e to be measured for several aliquots of the same sample, with subsequent statistical treatments of inter-aliquot differences yielding final D_e values with uncertainties $< 5\,\%$ (Mahan and DeWitt, 2019). The overall uncertainties for luminescence ages are usually quoted at 1 standard deviation and often range from 15 % to 20 % of the age for TL and from 5 % to 10 % for OSL or IRSL (Mahan and DeWitt, 2019). The lower limit of the luminescence dating range is decided only by the sensitivity of the devices measuring the signal and can be as low as 10 a (Ballarini et al., 2007). The upper limit of the dating range is determined by the dose rate and a saturation level of trapped electrons that differs between minerals. For conventional quartz OSL, this upper limit is typically around 150 to 200 ka, whereas for feldspar it ranges between 200 and 300 ka. However, the dose rate can significantly shift these limits. High dose rates in loess can cause quartz to saturate after 50 to 100 ka (e.g. Avram et al., 2020; Buylaert et al., 2007), while in settings with exceptionally low dose rates, ages of up to ~ 1 Ma can be obtained (e.g. Blechschmidt et al., 2009; Huntley et al., 1993; Rhodes et al., 2006). In addition to the age estimate and its confidence interval, luminescence publications will ideally be reported with the following information: a profile description of the sample site, both the internal and external dose rates for the sample and the values used to calculate them, a brief description of the luminescence measurement protocol used, the D_e value, and any information regarding fading rates and corrections. For more detailed discussions of luminescence methods and their applications to a wide range of geological contexts, readers are directed towards the reviews by Mahan and DeWitt (2019) and Tsukamoto (2025).

7.2 Luminescence dating in volcanic contexts

Volcanic contexts produce several sample materials for luminescence dating. The first of these are juvenile phenocrysts of quartz or feldspar, as well as glass, contained in lava or tephra (Fattahi and Stokes, 2003). The luminescence signal in these crystals starts at zero and will begin to accumulate after cooling to ambient temperatures, allowing luminescence

methods to estimate the time of eruption. In general, these materials should be approached with caution for luminescence dating, due to their propensity for severe anomalous fading (feldspar: Wintle, 1973; Huntley and Lamothe, 2001; Guérin and Visocekas, 2015; and quartz: Bonde et al., 2001; Tsukamoto et al., 2007). Nonetheless, specific protocols have been developed that measure non-fading emissions or those that fade at rates low enough to be corrected. For volcanic feldspar, these are the far-red TL emissions (∼ 710 nm) and pIRIR emissions measured at 300 °C (e.g. Visocekas et al., 2014; Tsukamoto et al., 2014; Biswas et al., 2013, 2015). For volcanic quartz, ages as old as 1.2 Ma have been measured through the red TL emissions (RTL, 620–630 nm) and isothermal RTL SAR protocols (Fattahi and Stokes, 2000; Tsukamoto et al., 2007; Ganzawa and Maeda, 2009). Volcanic glass has also been used for dating, particularly the 2–11 µm fraction (Berger, 1991, 1992), but further research is needed to establish the widespread applicability of this method. For more detailed discussions about dating these materials, please see the thorough discussion provided by Fattahi and Stokes (2000) and Bösken and Schmidt (2020). Additionally, juvenile zircon and olivine have been explored for luminescence dating, with inconclusive results (Clark-Balzan et al., 2021; Faïn et al., 1988).

As an alternative to juvenile material, quartz and feldspar of non-volcanic origin found in or adjacent to volcanic deposits are appealing target materials, as they are less likely to suffer from anomalous fading (Rufer et al., 2012). Examples of this kind of material are xenoliths contained within lava in scoria cones or flows (Shitaoka et al., 2014), xenolithic quartz crystals in basaltic tephra (Miallier et al., 1982; Sanzelle et al., 2000), baked rock or sediments below lava flows (Forman et al., 1994; Pilleyre et al., 1992; Robertson et al., 1996; Schmidt et al., 2017a), and finally fragments of crystalline basement contained in phreatic and phreatomagmatic deposits (Zöller and Blanchard, 2009; Preusser et al., 2011; Schmidt et al., 2017b). For these products, any pre-existing luminescence signal in the xenolithic material would be thermally reset by heat from the surrounding magma during transportation to the surface. The heating of xenoliths surrounded by magma was numerically modelled by Rufer et al. (2012) who found that the core of a 7 cm × 7 cm hand sample of granite surrounded by 800 °C (at the lower end of the range for magma/lava temperatures) would reach temperatures above 450 °C after only 260 s. They further tested this model in the laboratory and found that feldspars from both the surface and the core of a granite cube had their luminescence signals completely reset after 30 min. Thus, xenoliths allow direct dating of the eruption event. This signal resetting by heat is also the case for material baked under lava flows to depths of 30 cm (Pilleyre et al., 1992; Robertson et al., 1996). It is nonetheless recommended that these materials be measured with protocols that target non-fading signals (i.e. pIRIR) and are tested for fading. This is because of possible alteration to their luminescence behaviour due to pyrometamorphism at high temperatures. The resetting of the luminescence signal in country rock fragments from phreatic and phreatomagmatic deposits is not by heat but rather by thermally assisted mechanical stress from the shock of the explosion (Zöller et al., 2009; Preusser et al., 2011; Rufer et al., 2014). This is one of the few volcanic contexts where partial resetting could be encountered. The efficacy of this resetting is still debated, with some studies showing incomplete resetting of the signal (Preusser et al., 2011). For a more thorough discussion of these target materials and their potential issues, readers are directed to Rufer et al. (2012) and Bösken and Schmidt (2020).

7.3 Examples of luminescence dating applied to volcanism

As presented above, luminescence dating methods can be applied to a wide range of volcanic products and deposit types. One relatively common application of luminescence methods is dating non-volcanic sediments baked under lava flows. An example of this is a study by Pilleyre et al. (1992) on the use of the RTL peak at 380–395 °C to date quartz from sediments under the Tartaret, Boisséjour, and St Jacques lava flows in the Chaîne des Puys volcanic field, France. The RTL of quartz grains extracted from baked sediments under the respective lava flows were measured with a MAAD approach. For all samples, two dose response curves were derived which facilitated the calculation of a sensitisation factor for the extrapolated D_e value. The samples from Boisséjour and St Jacques both produced a large TL peak starting at 200 °C that overlapped with the high-temperature RTL peaks used for dating. This TL peak was removed with a 10 s preheat at 330 °C before performing the RTL measurements. The dosimetry for these samples was performed through flame photometry, in situ gamma dosimetry, and alpha counting. The resulting ages for the Boisséjour and St Jacques lava flows, 72 ± 7.5 and 60 ± 7 ka, respectively, agree with previously published TL ages for plagioclase feldspars from these lava flows (Guerin, 1983). The RTL age of 13.7 ± 0.8 ka for the Tartaret lava flow is older than previous radiocarbon ages for "black sediments" that are now known to produce age underestimates (Brousse et al., 1976; Camus et al., 1973).

In contrast to the previous example, luminescence methods can also be applied directly to juvenile volcanic products, despite their previously discussed susceptibility to anomalous fading. Anomalous fading is nearly ubiquitous in feldspar, but for quartz it has only been observed in volcanic products. A good example of this is Tsukamoto et al. (2007), who used OSL and isothermal RTL to measure volcanic quartz from Japan. These authors sampled juvenile quartz from two rhyolitic pyroclastic surge deposits on Kozu Island in the Izu Archipelago south of Tokyo and from a tephra in northern Nagano, central Japan. Radiocarbon ages related to the pyroclastic surges provided age control to the 20–30 ka range, while the position of the tephra in sequences around

Tokyo have been correlated to marine isotope stage 11. The dosimetry for these samples was calculated based on the concentration of U, Th, and K in bulk samples measured through neutron activation analysis. Both OSL and isothermal RTL were measured with suitable filter combinations to isolate the ultraviolet and the red (630–670 nm) emissions, respectively. SAR protocol measurements of the pyroclastic surge deposits produced D_e values that were found to be underestimates based on the dose rate and the radiocarbon age control. In response to this, a fading test that involved repeated OSL measurements of the same dose (30 Gy) after seven different time delays was performed. An average fading rate of 6.5 ± 0.5 % per decade was recorded for the OSL signal. Attempts to correct the previously measured D_e values were made following the method of Huntley and Lamothe (2001), but the corrected D_e values were still less than half of the expected amount. The RTL of this sample was also measured with a SAR protocol that yielded D_e values that were only slightly lower than the expected value. Finally, they measured the samples with an isothermal RTL SAR protocol that held the sample at stable temperatures between 300 and 400 °C for 500 s, allowing them to measure the decay of the signal over time. This approach has the benefit of making it easy to separate the isothermal RTL signal from thermal background noise. The D_e values obtained through isothermal RTL resulted in age estimates of 28.5 ± 1.2 ka for the pyroclastic deposits and 388 ± 25 ka for the tephra, which both agree with the independent age control.

A final example of how luminescence approaches can be used to date volcanic eruptions is the research by Preusser et al. (2011) on maars in the Eifel, Germany. Maars are generally the result of phreatic eruptions, in which case it is believed the luminescence signal is reset by mechanical stress from the explosive eruption style. Preusser et al. (2011) sampled unconsolidated tephra deposits from phreatic eruptions that consisted of fragmented Devonian sedimentary rock from Ulmener Maar and Meerfelder Maar in the Western Eifel. In addition, the authors sampled layers in the Laacher See tephra that were also rich in Devonian basement fragments. To determine D_e values, the quartz and feldspar fractions were measured with modified SAR OSL and IRSL protocols, respectively. For Meerfelder Maar, the average IRSL and OSL ages of 74.9 ± 5.0 and 74.9 ± 5.5 ka respectively agree perfectly and fit previously published TL ages (Zöller and Blanchard, 2009). The average IRSL of 11.6 ± 0.5 ka for Ulmener Maar agrees well with the available radiocarbon and varve-counting-based age control, while the average OSL age was slightly older at 14.2 ± 0.6 ka. Partial resetting of the OSL signal was dismissed as a possibility, as the distribution of D_e remained Gaussian. Differences in the signal resetting process due to mechanical stress between quartz and feldspar were considered as a possible explanation for this discrepancy. This mechanical resetting process is likely very different from thermal or optical resetting. The tephra samples from Laacher See in contrast produced OSL D_e values that were in saturation (i.e. not reset), and the IRSL D_e values showed a wide spread. The Laacher See is part of a more complex eruptive system, and the samples contained a larger percentage of juvenile volcanic material. This suggests that the explosions from phreatomagmatic eruptions involved in this tephra formation were not strong enough to reset the luminescence signals. This maar tephra study, among others mentioned above, demonstrates that luminescence methods can be used to date volcanic deposits lacking juvenile material, unlike U–Th or ^{40}K / ^{40}Ar and ^{40}Ar / ^{39}Ar approaches.

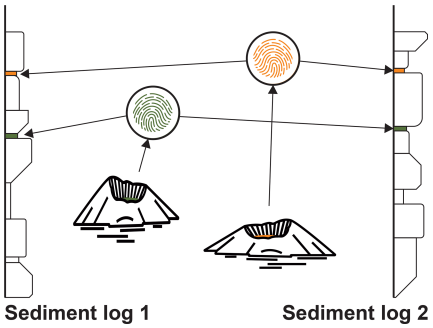

Figure 9. Schematic of geochemical fingerprinting of tephra layers to their source volcano.

8 Tephrochronology and counting methods

While the bulk of volcanic material is deposited close to the eruption centre, explosive eruptions can potentially spread tephra over large areas. Much of the erupted tephra is removed by erosion or weathering. However, some portions end up in lakes, bogs, or oceans, or on ice masses, where they can be preserved over long periods of time (e.g. Lowe, 2011; Lane et al., 2017). Tephra layers like these are also frequently found within dust deposits (i.e. loess: e.g. Busacca et al., 1992; Matsu'ura et al., 2011; Zens et al., 2017). While many tephra layers can be identified visually, individual volcanic particles can be identified using microscopes. Such cryptotephra (typically with a grain size of 25–120 µm) can travel thousands of kilometres. For identification and correlation to a specific eruption, geochemical signatures need to be established for each volcano/eruption and deposit (Fig. 9; Davies, 2015). While tephra layers are mainly used as marker horizons for regional correlations in palaeoenvironmental studies (e.g. Hall and Pilcher, 2002; Wastegård, 2005; Blockley et al., 2012; Davies et al., 2012), tephrochronology also has great potential for reconstructing recurrence intervals of large explosive eruptions (Ponomareva et al., 2015; Plunkett et al., 2015).

As the dating of certain types of volcanic material is challenging, the advantage of tephra layers is that they can be dated indirectly by determining the depositional age of the material in which they are embedded. Some of the methods mentioned above (radiocarbon, luminescence) can be used

for this purpose, and age-modelling approaches help to reduce the overall dating uncertainty related to individual samples (e.g. Lacourse and Gajewski, 2020). Very precise ages can be derived through the counting of annual layers that occur in ice cores (e.g. Abbott and Davies, 2012) or varved lake deposits (e.g. Lane et al., 2015). A key requirement of layer counting is that there must be clear evidence for the annual nature of the laminae. To obtain numerical chronologies, an anchor date is required, ideally by identifying the topmost varve formed during the year of coring. Consecutive layer counting can lead to dating uncertainties as small as a few per mille, the uncertainty being related to ambiguous laminations and hiatuses (Zolitschka et al., 2015). Two examples in the volcanological context are the Icelandic Vedde Ash which has been dated to $12\,140 \pm 40$ varve yr BP (with 1950 designated as "present") using the varved lake sediments of Meerfelder Maar in western Germany (Lane et al., 2013) and the Laacher See Tephra (Bogaard and Schmincke, 1985), which was dated to 12 880 varve yr BP (Brauer et al., 1999) and $13\,006 \pm 9$ yr BP by dendrochronology (Reinig et al., 2021).

A similar method is dendrochronology, which uses tree rings in large pieces of wood that grow at differing rates depending on environmental conditions, thus producing a characteristic pattern similar to barcodes (Biondi, 2014). Analysing this pattern allows volcanic eruptions to be identified through disturbances to tree growth by erupted volcanic products (e.g. Sheppard et al., 2008). However, in most cases the disturbance cannot be related independently to a specific eruption centre, therefore the method's usefulness for dating volcanism is limited.

9 Discussion and conclusions

The methods presented and reviewed in the present study are currently the best available for dating Quaternary volcanism. There are a few issues that should be of concern for all the methods. The first of these issues is establishing a clear connection between the sample being dated and an eruptive vent, which is not always straightforward. It is therefore essential that researchers provide evidence connecting the sample material they are dating to a specific volcano whenever possible. Four out of the five methods rely on measuring a temperature-dependent variable in the sample; Ar or He gas accumulation for $^{40}K / ^{40}Ar$ and $^{40}Ar / ^{39}Ar$, uranium series, and cosmogenic nuclide dating, along with trapped charge for luminescence. For these samples, it is important to confirm that they have not experienced a secondary heating event after being erupted, such as burial by a lava flow or a wildfire. This is of particular concern when dating polygenetic volcanoes due to the proximity of their products. A final concern for all methods is the importance of sampling deposits that have not been subsequently reworked or disturbed. The inclusion of detailed outcrop logs with published dates is of considerable benefit for addressing these three issues. Some of the methods are relatively easily applicable to a readily available volcanic product (e.g. K-bearing minerals in lava for $^{40}K / ^{40}Ar$ and $^{40}Ar / ^{39}Ar$ dating), while others require less common sample material (e.g. organic material for radiocarbon dating).

Several of the dating methods are based on relatively simple physical processes, but the proper measurement and calibration of the related parameters often present complications. All methods have their own advantages and disadvantages (Table 2). Additionally, they provide ages for slightly different phenomena related to volcanism; cooling below a certain temperature for $^{40}K / ^{40}Ar$ and $^{40}Ar / ^{39}Ar$, (U–Th) / He, and luminescence dating, surface exposure for cosmogenic nuclide dating, and the death of an organism for radiocarbon dating. For this reason, the best age estimates are those which are reproducible through at least two or more of these methods. It is essential for those using the ages provided for further research to understand the specific advantages and disadvantages of the methods. We advise against taking published ages from these methods at face value. Instead, we recommend that researchers perform a simple evaluation of ages, with the issues highlighted by this review in mind, before putting them to further use.

While some of the methods presented here were already established for the dating of volcanic events in the middle of the 20th century, all of these have seen substantial methodological improvements during the past decades. This has made it possible to produce more reliable and accurate age estimates for a wider range of volcanic deposits and products than before (during the 20th century). For example, while the underlying principle remains the same, the $^{40}Ar / ^{39}Ar$ method is far superior for the dating of Quaternary volcanism compared to the $^{40}K / ^{40}Ar$ method. Besides having a higher precision, $^{40}Ar / ^{39}Ar$ dating allows single crystal samples to be analysed with laser fusion or step heating, greatly improving its accuracy. For radiocarbon, the introduction of the AMS methodology and improved preparation procedures has allowed much smaller samples to be measured in less time. This goes as far as using compound-specific analysis of fatty acids (Yamamoto et al., 2024). In addition, substantial work has been done to improve the radiocarbon calibration curves. For uranium series dating, zircon double dating has allowed the direct determination of the onset and duration of pre-eruptive zircon crystallisation. Furthermore, the approach approximates the timing of cooling which in the case of rapidly quenched tephra allows researchers to better constrain the age of the eruption. Cosmogenic nuclide dating was only established in the 1990s and already allows the direct dating of landforms related to volcanic activity. While luminescence dating of volcanic products has been tested since the 1960s, its wide implementation has been hampered by the presence of anomalous fading in minerals of volcanic origin. This problem has been approached by using signals that are

Table 2. Summary of the key characteristics of radiometric methods used to date volcanic events.

Method	Material	Dated event	Age range	Potential problems
^{40}K / ^{40}Ar, ^{40}Ar / ^{39}Ar	K-bearing minerals in basaltic to felsic lavas	Cooling below ca. 500–150 °C	Some ka to ∞	Ar diffusion, inherited/excess Ar, atomic recoil
Radiocarbon	Organic material in or adjacent to volcanic products	Death of organism, may pre- or post-date volcanism	Up to 55 ka	Reservoir effects, reworking, contamination, plateaus in calibration curves
Uranium series	Zircon and other accessory minerals	Mineral crystallisation (U–Th dis.), cooling during ascent ((U–Th) / He)	Some ka to > 100 ka (U–Th dis.); some ka to ∞ ((U–Th) / He) and ZDD); 1 Ma to ∞ (U–Th–Pb)	Duration of crystallisation, disequilibrium, atomic recoil
Cosmogenic nuclides	Quartz, olivine, pyroxene, carbonates, feldspar, whole rock	Exposure at surface	Centuries to > 10 Ma (depending on TCN)	Inherited nuclides, erosion, surface shielding, calculation of regional production rates
Luminescence	Quartz, feldspar	Cooling to ambient temperatures (below ca. 300 °C)	Decades to some 100 ka	Fading, partial resetting

less or even not affected by this phenomenon, in particular RTL and pIRIR.

Despite the enormous efforts regarding methodological developments, there are cases such as the age of the Thera eruption where methodological issues remain unsolved. In the future, developments in analytical equipment and procedures will likely further improve the accuracy and precision of the methods summarised in this paper. This, together with a push for a general increase in the number of dated events worldwide, will lead to an improved foundation for volcanic hazard assessments.

Data availability. All data used to produce figures can be found through the provided references.

Author contributions. FP and DM conceptualised the paper. FP and WM acquired funding. WM drafted most of the paper and the figures. VM, FP, and ES drafted the K / Ar + Ar / Ar, radiocarbon, and cosmogenic nuclide dating sections, respectively. WM, DM, and FP contributed to the review and editing of the final version of the paper.

Competing interests. The contact author has declared that none of the authors has any competing interests.

Disclaimer. Publisher's note: Copernicus Publications remains neutral with regard to jurisdictional claims made in the text, published maps, institutional affiliations, or any other geographical representation in this paper. The authors bear the ultimate responsibility for providing appropriate place names. Views expressed in the text are those of the authors and do not necessarily reflect the views of the publisher.

Acknowledgements. The authors would like to thank Benjamin van Wyk de Vries for fruitful discussions in the early stages of planning this paper. Additional thanks are due to Wolfgang Sielbel for support in compiling information for the U-series portion. Finally, we thank Christoph Schmidt and the anonymous reviewer for their detailed and constructive comments that resulted in an improved paper.

Financial support. This study was financially supported by the German Research Foundation (DFG) through the "Reconstructing the Late Quaternary eruption history of the Chaîne des Puys, France, using modern luminescence dating approaches" project granted to Frank Preusser (project no. 490668505).

This open-access publication was funded by the University of Freiburg.

Review statement. This paper was edited by Markus Fuchs and reviewed by Christoph Schmidt and one anonymous referee.

References

Abbott, P. M. and Davies, S. M.: Volcanism and the Greenland ice-cores: the tephra record, Earth Sci. Rev., 115, 173–191, https://doi.org/10.1016/j.earscirev.2012.09.001, 2012.

Aitken, M. J.: Thermoluminescence dating: Past progress and future trends, Nucl. Tracks Rad. Meas., 10, 3–6, https://doi.org/10.1016/0735-245X(85)90003-1, 1985.

Aitken, M. J.: Introduction to Optical Dating: The Dating of Quaternary Sediments by the Use of Photon-stimulated Luminescence, Clarendon Press, 282 pp., ISBN 978-0-19-158927-0, 1998.

Alcalá-Reygosa, J., Palacios, D., Schimmelpfennig, I., Vázquez-Selem, L., García-Sancho, L., Franco-Ramos, O., Villanueva, J., Zamorano, J. J., Aumaître, G., Bourlès, D., and Keddadouche, K.: Dating late Holocene lava flows in Pico de Orizaba (Mexico) by means of in situ-produced cosmogenic ^{36}Cl, lichenometry and dendrochronology, Quat. Geochronol., 47, 93–106, https://doi.org/10.1016/j.quageo.2018.05.011, 2018.

Aldrich, L. T. and Nier, A. O.: Argon-40 in Potassium Minerals, Phys. Rev., 74, 876–877, https://doi.org/10.1103/PhysRev.74.876, 1948.

Allegre, C. L.: ^{230}Th dating of volcanic rocks: A comment, Earth Planet. Sci. Lett., 5, 209–210, https://doi.org/10.1016/S0012-821X(68)80042-1, 1968.

Alves, E. Q., Macario, K., Ascough, P., and Bronk Ramsey, C.: The Worldwide Marine Radiocarbon Reservoir Effect: Definitions, Mechanisms, and Prospects, Rev. Geophys., 56, 278–305, https://doi.org/10.1002/2017RG000588, 2018.

Auclair, M., Lamothe, M., and Huot, S.: Measurement of anomalous fading for feldspar IRSL using SAR, Radiat. Meas., 37, 487–492, https://doi.org/10.1016/S1350-4487(03)00018-0, 2003.

Avram, A., Constantin, D., Veres, D., Kelemen, S., Obreht, I., Hambach, U., Marković, S. B., and Timar-Gabor, A.: Testing polymineral post-IR IRSL and quartz SAR-OSL protocols on Middle to Late Pleistocene loess at Batajnica, Serbia, Boreas, 49, 615–633, https://doi.org/10.1111/bor.12442, 2020.

Baksi, A. K.: Geochronological studies on whole-rock basalts, Deccan Traps, India: evaluation of the timing of volcanism relative to the K-T boundary, Earth Planet. Sci. Lett., 121, 43–56, https://doi.org/10.1016/0012-821X(94)90030-2, 1994.

Balco, G., Briner, J., Finkel, R. C., Rayburn, J. A., Ridge, J. C., and Schaefer, J. M.: Regional beryllium-10 production rate calibration for late-glacial northeastern North America, Quat. Geochronol., 4, 93–107, https://doi.org/10.1016/j.quageo.2008.09.001, 2009.

Balco, G., Stone, J., Śliwiński, M., and Todd, C.: Features of the glacial history of the Transantarctic Mountains inferred from cosmogenic ^{26}Al, ^{10}Be and ^{21}Ne concentrations in bedrock surfaces, Antarct. Sci., 26, 708–723, https://doi.org/10.1017/S0954102014000261, 2014.

Ballarini, M., Wallinga, J., Wintle, A., and Bos, A.: A modified SAR protocol for optical dating of individual grains from young quartz samples, Radiat. Meas., 42, 360–369, https://doi.org/10.1016/j.radmeas.2006.12.016, 2007.

Balter-Kennedy, A., Bromley, G., Balco, G., Thomas, H., and Jackson, M. S.: A 14.5-million-year record of East Antarctic Ice Sheet fluctuations from the central Transantarctic Mountains, constrained with cosmogenic ^{3}He, ^{10}Be, ^{21}Ne, and ^{26}Al, The Cryosphere, 14, 2647–2672, https://doi.org/10.5194/tc-14-2647-2020, 2020.

Balter-Kennedy, A., Schaefer, J. M., Schwartz, R., Lamp, J. L., Penrose, L., Middleton, J., Hanley, J., Tibari, B., Blard, P.-H., Winckler, G., Hidy, A. J., and Balco, G.: Cosmogenic ^{10}Be in pyroxene: laboratory progress, production rate systematics, and application of the ^{10}Be–^{3}He nuclide pair in the Antarctic Dry Valleys, Geochronology, 5, 301–321, https://doi.org/10.5194/gchron-5-301-2023, 2023.

Becquerel, H.: Émission de radiations nouvelles par l'uranium métallique, Gauthier-Villars, Paris, France, https://www.academie-sciences.fr/pdf/dossiers/Becquerel/Becquerel_pdf/CR1896_p1086.pdf (last access: 14 September 2025), 1896.

Berger, G. W.: The use of glass for dating volcanic ash by thermoluminescence, J. Geophys. Res.-Sol. Ea., 96, 19705–19720, https://doi.org/10.1029/91JB01899, 1991.

Berger, G. W.: Dating volcanic ash by use of thermoluminescence, Geology, 20, 11–14, https://doi.org/10.1130/0091-7613(1992)020<0011:DVABUO>2.3.CO;2, 1992.

Bietak, M.: Science versus Archaeology: Problems and Consequences of High Aegean Chronology, in: The synchronisation of civilisations in the Eastern Mediterranean in the second millennium B.C.: 2, Proceedings of the SCIEM 2000 – EuroConference, Haindorf, 23–34, ISBN 3-7001-3176-3, 2003.

Bietak, M.: Radiocarbon and the date of the Thera eruption, Antiquity, 88, 277–282, https://doi.org/10.1017/S0003598X00050389, 2014.

Biondi, F.: Dendrochronology, Volcanic Eruptions, in: Encyclopedia of Earth Sciences Series, Springer, 1–11, https://doi.org/10.1007/978-94-007-6326-5_24-1, 2014.

Biswas, R., Williams, M., Raj, R., Juyal, N., and Singhvi, A.: Methodological studies on luminescence dating of volcanic ashes, Quat. Geochronol., 17, 14–25, https://doi.org/10.1016/j.quageo.2013.03.004, 2013.

Biswas, R., Toyoda, S., Takada, M., and Shitaoka, Y.: Multiple approaches to date Japanese marker tephras using optical and ESR methods, Quat. Geochronol., 30, 350–356, https://doi.org/10.1016/j.quageo.2015.01.004, 2015.

Blard, P.-H.: Cosmogenic ^{3}He in terrestrial rocks: A review, Chem. Geol., 586, 120543, https://doi.org/10.1016/j.chemgeo.2021.120543, 2021.

Blechschmidt, I., Matter, A., Preusser, F., and Rieke-Zapp, D.: Monsoon triggered formation of Quaternary alluvial megafans in the interior of Oman, Geomorphology, 110, 128–139, https://doi.org/10.1016/j.geomorph.2009.04.002, 2009.

Blockley, S. P. E., Lane, C. S., Hardiman, M., Rasmussen, S. O., Seierstad, I. K., Steffensen, J. P., Svensson, A., Lotter, A. F., Turney, C. S. M., and Bronk Ramsey, C.: Synchronisation of palaeoenvironmental records over the last 60 000 years, and an extended INTIMATE1 event stratigraphy to 48 000 b2k, Quat. Sci. Rev., 36, 2–10, https://doi.org/10.1016/j.quascirev.2011.09.017, 2012.

Bogaard, P. V. D. and Schmincke, H.-U.: Laacher See Tephra: A widespread isochronous late Quaternary tephra layer in central and northern Europe, Geol. Soc. Am. Bull., 96, 1554–1571, https://doi.org/10.1130/0016-7606(1985)96<1554:LSTAWI>2.0.CO;2, 1985.

Bonde, A., Murray, A., and Friedrich, W. L.: Santorini: Luminescence dating of a volcanic province using quartz?, Quat. Sci. Rev., 20, 789–793, https://doi.org/10.1016/S0277-3791(00)00034-2, 2001.

Bösken, J. J. and Schmidt, C.: Direct and indirect luminescence dating of tephra: A review, J. Quat. Sci., 35, 39–53, https://doi.org/10.1002/jqs.3160, 2020.

Bourdon, B. and Sims, K. W. W.: U-series Constraints on Intraplate Basaltic Magmatism, Rev. Mineral. Geochem., 52, 215–254, https://doi.org/10.2113/0520215, 2003.

Bourdon, B., Zindler, A., and Wörner, G.: Evolution of the Laacher See magma chamber: Evidence from SIMS and TIMS measurements of U–Th disequilibria in minerals and glasses, Earth Planet. Sci. Lett., 126, 75–90, https://doi.org/10.1016/0012-821X(94)90243-7, 1994.

Bourdon, B., Henderson, G. M., Lundstrom, C. C., and Turner, S.: Uranium-series Geochemistry, Walter de Gruyter GmbH & Co KG, 676 pp., ISBN 978-1-5015-0930-8, 2018.

Bowen, N. L.: The Reaction Principle in Petrogenesis, J. Geol., 30, 177–198, https://doi.org/10.1086/622871, 1922.

Brauer, A., Endres, C., Günter, C., Litt, T., Stebich, M., and Negendank, J. F. W.: High resolution sediment and vegetation responses to Younger Dryas climate change in varved lake sediments from Meerfelder Maar, Germany, Quat. Sci. Rev., 18, 321–329, https://doi.org/10.1016/S0277-3791(98)00084-5, 1999.

Brock, F., Higham, T., Ditchfield, P., and Bronk Ramsey, C.: Current Pretreatment Methods for AMS Radiocarbon Dating at the Oxford Radiocarbon Accelerator Unit (ORAU), Radiocarbon, 52, 103–112, https://doi.org/10.1017/S0033822200045069, 2010.

Bromley, G. R. M., Thouret, J.-C., Schimmelpfennig, I., Mariño, J., Valdivia, D., Rademaker, K., del Pilar Vivanco Lopez, S., Team, A., Aumaître, G., Bourlès, D., and Keddadouche, K.: In situ cosmogenic ^{3}He and ^{36}Cl and radiocarbon dating of volcanic deposits refine the Pleistocene and Holocene eruption chronology of SW Peru, Bull. Volcanol., 81, 64, https://doi.org/10.1007/s00445-019-1325-6, 2019.

Bronk Ramsey, C., Manning, S. W., and Galimberti, M.: Dating the Volcanic Eruption at Thera, Radiocarbon, 46, 325–344, https://doi.org/10.1017/S0033822200039631, 2004.

Brousse, R., Maury, R., and Santoire, J. P.: L'Age de la coulée du Tartaret, C. R. Acad. Sci. Paris, Sér. D, 282, 531–532, 1976.

Brown, S., Sparks, R., Mee, K., Vye-Brown, C., Ilyinskaya, E., Jenkins, S., and Loughlin, S.: Appendix B Country and regional profiles of volcanic hazard and risk, in: Global Volcanic Hazards and Risk, Cambridge University Press, Cambridge, 1–789, https://doi.org/10.1017/cbo9781316276273, 2015.

Bruins, H. J. and van der Plicht, J.: The Minoan Thera eruption predates Pharaoh Ahmose: Radiocarbon dating of Egyptian 17th to early 18th Dynasty museum objects, PLOS ONE, 20, https://doi.org/10.1371/journal.pone.0330702, 2025.

Busacca, A. J., Nelstead, K. T., McDonald, E. V., and Purser, M. D.: Correlation of Distal Tephra Layers in Loess in the Channeled Scabland and Palouse of Washington state, Quat. Res., 37, 281–303, https://doi.org/10.1016/0033-5894(92)90067-S, 1992.

Buylaert, J., Jain, M., Murray, A. S., Thomsen, K. J., Thiel, C., and Sohbati, R.: A robust feldspar luminescence dating method for Middle and Late Pleistocene sediments, Boreas, 41, 435–451, https://doi.org/10.1111/j.1502-3885.2012.00248.x, 2012.

Buylaert, J. P., Vandenberghe, D., Murray, A. S., Huot, S., De Corte, F., and Van Den Haute, P.: Luminescence dating of old (> 70 ka) Chinese loess: A comparison of single-aliquot OSL and IRSL techniques, Quat. Geochronol., 2, 9–14, https://doi.org/10.1016/j.quageo.2006.05.028, 2007.

Buylaert, J.-P., Murray, A. S., Thomsen, K. J., and Jain, M.: Testing the potential of an elevated temperature IRSL signal from K-feldspar, Radiat. Meas., 44, 560–565, https://doi.org/10.1016/j.radmeas.2009.02.007, 2009.

Calderoni, G. and Turi, B.: Major Constraints on the Use of Radiocarbon Dating for Tephrochronology, Quatern. Int., 47–48, 153–159, https://doi.org/10.1016/S1040-6182(97)00082-7, 1998.

Camus, G., Herve, A., Kieffer, G., Mergoil, J., and Vincent, P. M.: Mise au point sur la dynamisme at la chronologie des volcans holocènes de la région de Besse-en-Chandesse, C. R. Acad. Sci. Paris, 277, 629–632, 1973.

Cañón-Tapia, E.: Reappraisal of the significance of volcanic fields, J. Volcanol. Geotherm. Res., 310, 26–38, https://doi.org/10.1016/j.jvolgeores.2015.11.010, 2016.

Capra, L., Macías, J. L., Espíndola, J. M., and Siebe, C.: Holocene plinian eruption of La Virgen volcano, Baja California, Mexico, J. Volcanol. Geotherm. Res., 80, 239–266, https://doi.org/10.1016/S0377-0273(97)00049-8, 1998.

Cerrai, E.: Il Metodo ionio/urano per la determinazione dell'eta' di minerali vulcanici recenti, Rend. Soc. Mineral. Ital., 21, 47–62, 1965.

Cersoy, S., Zazzo, A., Rofes, J., Tresset, A., Zirah, S., Gauthier, C., Kaltnecker, E., Thil, F., and Tisnerat-Laborde, N.: Radiocarbon dating minute amounts of bone (3–60 mg) with ECHoMICADAS, Sci. Rep., 7, 7141, https://doi.org/10.1038/s41598-017-07645-3, 2017.

Cheng, H., Lawrence Edwards, R., Shen, C.-C., Polyak, V. J., Asmerom, Y., Woodhead, J., Hellstrom, J., Wang, Y., Kong, X., Spötl, C., Wang, X., and Calvin Alexander, E.: Improvements in ^{230}Th dating, ^{230}Th and ^{234}U half-life values, and U–Th isotopic measurements by multi-collector inductively coupled plasma mass spectrometry, Earth Planet. Sci. Lett., 371–372, 82–91, https://doi.org/10.1016/j.epsl.2013.04.006, 2013.

Chernyshev, I. V., Lebedev, V. A., and Arakelyants, M. M.: K-Ar dating of quaternary volcanics: Methodology and interpretation of results, Petrology, 14, 62–80, https://doi.org/10.1134/S0869591106010061, 2006.

Clark-Balzan, L., May, V. R., and Preusser, F.: Luminescence Characteristics of Intraplate-Derived Olivines, Geochronometria, 48, 73–94, https://doi.org/10.2478/geochr-2021-0006, 2021.

Condomines, M.: Dating recent volcanic rocks through ^{230}Th–^{238}U disequilibrium in accessory minerals: Example of the Puy de Dôme (French Massif Central), Geology, 25, 375–378, https://doi.org/10.1130/0091-7613(1997)025<0375:DRVRTT>2.3.CO;2, 1997.

Condomines, M., Gauthier, P.-J., and Sigmarsson, O.: Timescales of Magma Chamber Processes and Dating of Young Volcanic Rocks, Rev. Mineral. Geochem., 52, 125–174, https://doi.org/10.2113/0520125, 2003.

Connor, C. B., Stamatakos, J. A., Ferrill, D. A., Hill, B. E., Ofoegbu, G. I., Conway, F. M., Sagar, B., and Trapp, J.: Geologic factors controlling patterns of small-volume basaltic volcanism: Application to a volcanic hazards assessment at Yucca

Mountain, Nevada, J. Geophys. Res.-Sol. Ea., 105, 417–432, https://doi.org/10.1029/1999JB900353, 2000.

Cox, A.: Analysis of Present Geomagnetic Field for Comparison with Paleomagnetic Results, J. Geomag. Geoelec., 13, 101–112, https://doi.org/10.5636/jgg.13.101, 1962.

Craig, H.: The Natural Distribution of Radiocarbon and the Exchange Time of Carbon Dioxide Between Atmosphere and Sea, Tellus, 9, 1–17, https://doi.org/10.1111/j.2153-3490.1957.tb01848.x, 1957.

Curie, M. A.: du texte: Recherches sur les substances radioactives/par Mme Sklodowska Curie, Gauthier-Villars, Paris, ark:/12148/btv1b8626316v, 1903.

Daniels, F., Boyd, C. A., and Saunders, D. F.: Thermoluminescence as a research tool, Science, 117, 343–349, https://doi.org/10.1126/science.117.3040.343, 1953.

Danišík, M., Shane, P., Schmitt, A. K., Hogg, A., Santos, G. M., Storm, S., Evans, N. J., Keith Fifield, L., and Lindsay, J. M.: Re-anchoring the late Pleistocene tephrochronology of New Zealand based on concordant radiocarbon ages and combined $^{238}U/^{230}Th$ disequilibrium and (U–Th) / He zircon ages, Earth Planet. Sci. Lett., 349–350, 240–250, https://doi.org/10.1016/j.epsl.2012.06.041, 2012.

Danišík, M., Schmitt, A. K., Stockli, D. F., Lovera, O. M., Dunkl, I., and Evans, N. J.: Application of combined U–Th-disequilibrium/U–Pb and (U–Th) / He zircon dating to tephrochronology, Quat. Geochronol., 40, 23–32, https://doi.org/10.1016/j.quageo.2016.07.005, 2017.

Davies, S. M.: Cryptotephras: the revolution in correlation and precision dating, J. Quat. Sci., 30, 114–130, https://doi.org/10.1002/jqs.2766, 2015.

Davies, S. M., Abbott, P. M., Pearce, N. J. G., Wastegård, S., and Blockley, S. P. E.: Integrating the INTIMATE records using tephrochronology: rising to the challenge, Quat. Sci. Rev., 36, 11–27, https://doi.org/10.1016/j.quascirev.2011.04.005, 2012.

Deevey, E. S., Gross, M. S., Hutchinson, G. E., and Kraybill, H. L.: The natural c14 contents of materials from hard-water lakes, P. Natl. Acad. Sci. USA, 40, 285–288, https://doi.org/10.1073/pnas.40.5.285, 1954.

Delunel, R., Bourlès, D. L., van der Beek, P. A., Schlunegger, F., Leya, I., Masarik, J., and Paquet, E.: Snow shielding factors for cosmogenic nuclide dating inferred from long-term neutron detector monitoring, Quat. Geochronol., 24, 16–26, https://doi.org/10.1016/j.quageo.2014.07.003, 2014.

Doll, P., Eaves, S. R., Kennedy, B. M., Blard, P.-H., Nichols, A. R. L., Leonard, G. S., Townsend, D. B., Cole, J. W., Conway, C. E., Baldwin, S., Fénisse, G., Zimmermann, L., and Tibari, B.: Cosmogenic ^{3}He chronology of postglacial lava flows at Mt Ruapehu, Aotearoa / New Zealand, Geochronology, 6, 365–395, https://doi.org/10.5194/gchron-6-365-2024, 2024.

Duller, G. A. T.: A new method for the analysis of infrared stimulated luminescence data from potassium feldspars, Radiat. Meas., 23, 281–285, https://doi.org/10.1016/1350-4487(94)90053-1, 1994.

Duller, G. A. T.: Luminescence dating using single aliquots: methods and applications, Radiat. Meas., 24, 217–226, https://doi.org/10.1016/1350-4487(95)00150-D, 1995.

Duller, G. A. T.: What date is it? Should there be an agreed datum for luminescence ages?, Ancient TL, 29, 1–3, https://doi.org/10.26034/la.atl.2011.442, 2011.

Dunai, T. J.: Cosmogenic Nuclides: Principles, Concepts and Applications in the Earth Surface Sciences, Cambridge University Press, 199 pp., ISBN 978-1-139-48718-4, 2010.

Dunai, T. J. and Stuart, F. M.: Reporting of cosmogenic nuclide data for exposure age and erosion rate determinations, Quat. Geochronol., 4, 437–440, https://doi.org/10.1016/j.quageo.2009.04.003, 2009.

Dutton, A., Rubin, K. H., McLean, N., Bowring, J., Bard, E., Edwards, R. L., Henderson, G. M., Reid, M. R., Richards, D. A., Sims, K. W. W., Walker, J. D., and Yokoyama, Y.: Data reporting standards for publication of U-series data for geochronology and timescale assessment in the earth sciences, Quat. Geochronol., 39, 142–149, https://doi.org/10.1016/j.quageo.2017.03.001, 2017.

Erdil, P., Kuitems, M., Scifo, A., Brown, D., and Dee, M. W.: Investigating potential radiocarbon anomalies around the time of the Minoan eruption of Thera: A new high-resolution dataset from Groningen, Radiocarbon, 1–17, https://doi.org/10.1017/RDC.2025.10186, 2026.

Espanon, V. R., Honda, M., and Chivas, A. R.: Cosmogenic ^{3}He and ^{21}Ne surface exposure dating of young basalts from Southern Mendoza, Argentina, Quat. Geochronol., 19, 76–86, https://doi.org/10.1016/j.quageo.2013.09.002, 2014.

Evin, J.: Les datations par le radiocarbone en géologie et en archéologie, Fiabilité de la méthode selon l'origine et l'état des matériaux, Docum. Lab. Géol. Lyon, 122, 3–99, https://www.persee.fr/doc/geoly_0750-6635_1992_mon_122_1 (last access: 27 October 2025), 1992.

Fabel, D., Stroeven, A. P., Harbor, J., Kleman, J., Elmore, D., and Fink, D.: Landscape preservation under Fennoscandian ice sheets determined from in situ produced ^{10}Be and ^{26}Al, Earth Planet. Sci. Lett., 201, 397–406, https://doi.org/10.1016/S0012-821X(02)00714-8, 2002.

Faïn, J., Miallier, D., Montret, M., and Sanzelle, S.: Zircon dating: Regeneration and evaluation of the external dose, Int. J. Radiat. Appl. Instrum. Part D, 14, 333–337, https://doi.org/10.1016/1359-0189(88)90085-4, 1988.

Faïn, J., Erramli, H., Miallier, D., Montret, M., and Sanzelle, S.: Datation par Thermoluminescence d'un Appareil Volcanique Trachytique: Le Puy de Dôme, in: Datation et Charactérisation des Millieux Pléistocènes, Centre National de la Recherche Scientifique, Paris, 53–62, ISBN 2-222-094567-3, 1991.

Farley, K. A.: (U–Th) / He Dating: Techniques, Calibrations, and Applications, Rev. Mineral. Geochem., 47, 819–844, https://doi.org/10.2138/rmg.2002.47.18, 2002.

Farley, K. A., Wolf, R. A., and Silver, L. T.: The effects of long alpha-stopping distances on (U–Th) / He ages, Geochim. Cosmochim. Acta, 60, 4223–4229, https://doi.org/10.1016/S0016-7037(96)00193-7, 1996.

Farley, K. A., Kohn, B. P., and Pillans, B.: The effects of secular disequilibrium on (U–Th) / He systematics and dating of Quaternary volcanic zircon and apatite, Earth Planet. Sci. Lett., 201, 117–125, https://doi.org/10.1016/S0012-821X(02)00659-3, 2002.

Fattahi, M. and Stokes, S.: Extending the time range of luminescence dating using red TL (RTL) from volcanic quartz, Radiat. Meas., 32, 479–485, https://doi.org/10.1016/S1350-4487(00)00105-0, 2000.

Fattahi, M. and Stokes, S.: Dating volcanic and related sediments by luminescence methods: a review, Earth Sci. Rev., 62, 229–264, https://doi.org/10.1016/S0012-8252(02)00159-9, 2003.

Fenton, C., Webb, R., Pearthree, P., Cerling, T., Poreda, and Nash, B.: Cosmogenic ^{3}He dating of western Grand Canyon basalts: implications for Quaternary incision of the Colorado River, in: Colorado River origin and evolution, Grand Canyon Association, Grand Canyon, 147–152, ISBN 9780938216797, 2004.

Fenton, C. R., Niedermann, S., Goethals, M. M., Schneider, B., and Wijbrans, J.: Evaluation of cosmogenic ^{3}He and ^{21}Ne production rates in olivine and pyroxene from two Pleistocene basalt flows, western Grand Canyon, AZ, USA, Quat. Geochronol., 4, 475–492, https://doi.org/10.1016/j.quageo.2009.08.002, 2009.

Féraud, G. and Courtillot, V.: Comment on: "did Deccan volcanism pre-date the Cretaceous-Tertiary transition?", Earth Planet. Sci. Lett., 122, 259–262, https://doi.org/10.1016/0012-821X(94)90068-X, 1994.

Fleck, R. J., Hagstrum, J. T., Calvert, A. T., Evarts, R. C., and Conrey, R. M.: ^{40}Ar / ^{39}Ar geochronology, paleomagnetism, and evolution of the Boring volcanic field, Oregon and Washington, USA, Geosphere, 10, 1283–1314, https://doi.org/10.1130/GES00985.1, 2014.

Fleischer, R. L., Price, P. B., and Walker, R. M.: Fission-track ages of zircons, J. Geophys. Res., 69, 4885–4888, https://doi.org/10.1029/JZ069i022p04885, 1964.

Forman, S. L., Pierson, J., Smith, R. P., Hackett, W. R., and Valentine, G.: Assessing the accuracy of thermoluminescence for dating baked sediments beneath late Quaternary lava flows, Snake River Plain, Idaho, J. Geophys. Res.-Sol. Ea., 99, 15569–15576, https://doi.org/10.1029/94JB00806, 1994.

Friedrich, R., Kromer, B., Wacker, L., Olsen, J., Remmele, S., Lindauer, S., Land, A., and Pearson, C.: A New Annual ^{14}C Dataset for Calibrating the Thera Eruption, Radiocarbon, 62, 953–961, https://doi.org/10.1017/RDC.2020.33, 2020.

Friedrich, W. L., Kromer, B., Friedrich, M., Heinemeier, J., Pfeiffer, T., and Talamo, S.: Santorini Eruption Radiocarbon Dated to 1627–1600 B.C., Science, 312, 548–548, https://doi.org/10.1126/science.1125087, 2006.

Fukuoka, T. and Kigoshi, K.: Discordant Io-ages and the uranium and thorium distribution between zircon and host rocks, Geochem. J., 8, 117–122, https://doi.org/10.2343/geochemj.8.117, 1974.

Galbraith, R. F. and Roberts, R. G.: Statistical aspects of equivalent dose and error calculation and display in OSL dating: An overview and some recommendations, Quat. Geochronol., 11, 1–27, https://doi.org/10.1016/j.quageo.2012.04.020, 2012.

Ganzawa, Y. and Maeda, M.: 390–410 °C isothermal red thermoluminescence (IRTL) dating of volcanic quartz using the SAR method, Radiat. Meas., 44, 517–522, https://doi.org/10.1016/j.radmeas.2009.06.005, 2009.

Geyh, M. A.: Bomb Radiocarbon Dating of Animal Tissues and Hair, Radiocarbon, 43, 723–730, https://doi.org/10.1017/S0033822200041382, 2001.

Gill, E.: Potassium/argon age of basalt in floor of Hopkins River, Allansford, SW Victoria, Australia, Vic. Nat., 98, 188–190, 1981.

Gillen, D., Honda, M., Chivas, A. R., Yatsevich, I., Patterson, D. B., and Carr, P. F.: Cosmogenic ^{21}Ne exposure dating of young basaltic lava flows from the Newer Volcanic Province, western Victoria, Australia, Quat. Geochronol., 5, 1–9, https://doi.org/10.1016/j.quageo.2009.08.004, 2010.

Gleadow, A. J. W. and Duddy, I. R.: A natural long-term track annealing experiment for apatite, Nuclear Tracks, 5, 169–174, https://doi.org/10.1016/0191-278X(81)90039-1, 1981.

Gordon, J. E. and Harkness, D. D.: Magnitude and geographic variation of the radiocarbon content in Antarctic marine life: Implications for reservoir corrections in radiocarbon dating, Quaternary Sci. Rev., 11, 697–708, https://doi.org/10.1016/0277-3791(92)90078-M, 1992.

Gosse, J. C. and Phillips, F. M.: Terrestrial in situ cosmogenic nuclides: theory and application, Quaternary Sci. Rev., 20, 1475–1560, https://doi.org/10.1016/S0277-3791(00)00171-2, 2001.

Grün, R.: Amino Acid Racemization Dating, Encyclopedia of Archaeology, 429–433, https://doi.org/10.1016/B978-012373962-9.00006-6, 2008.

Guerin, G.: La thermoluminescence des plagioclases: methode de datation du volcanisme: applications au domaine volcanique francais: Chaine des Puys, mont Dore et Cezallier, Bas Vivarais, Universite Pierre et Marie Curie, https://www.worldcat.org/oclc/38676602 (last access: 24 June 2026), 1983.

Guérin, G. and Visocekas, R.: Volcanic feldspars anomalous fading: Evidence for two different mechanisms, Radiat. Meas., 81, 218–223, https://doi.org/10.1016/j.radmeas.2015.08.009, 2015.

Guilderson, T. P., Reimer, P. J., and Brown, T. A.: The Boon and Bane of Radiocarbon Dating, Science, 307, 362–364, https://doi.org/10.1126/science.1104164, 2005.

Guillou, H., Carracedo, J. C., and Day, S. J.: Dating of the Upper Pleistocene–Holocene volcanic activity of La Palma using the unspiked K–Ar technique, J. Volcanol. Geotherm. Res., 86, 137–149, https://doi.org/10.1016/S0377-0273(98)00074-2, 1998.

Hajdas, I.: Radiocarbon dating and its applications in Quaternary studies, E&G Quaternary Sci. J., 57, 2–24, https://doi.org/10.3285/eg.57.1-2.1, 2008.

Hajdas, I., Ascough, P., Garnett, M. H., Fallon, S. J., Pearson, C. L., Quarta, G., Spalding, K. L., Yamaguchi, H., and Yoneda, M.: Radiocarbon dating, Nat. Rev. Methods Primers, 1, 62, https://doi.org/10.1038/s43586-021-00058-7, 2021.

Hall, V. A. and Pilcher, J. R.: Late-Quaternary Icelandic tephras in Ireland and Great Britain: detection, characterization and usefulness, Holocene, 12, 223–230, https://doi.org/10.1191/0959683602hl538rr, 2002.

Hamilton, W. D., Haselgrove, C., and Gosden, C.: The impact of Bayesian chronologies on the British Iron Age, World Archaeol., 47, 642–660, https://doi.org/10.1080/00438243.2015.1053976, 2015.

Harrison, T. M.: Diffusion of ^{40}Ar in hornblende, Contr. Mineral. Petrol., 78, 324–331, https://doi.org/10.1007/BF00398927, 1982.

Hausback, B. P. and Abrams, M. J.: Plinian eruption of La Virgen Tephra, Volcán Las Tres Virgenes, Baja California Sur, Mexico, Eos, 77, 813–814, 1996.

Haynes, W. (Ed.): CRC Handbook Of Chemistry And Physics, 97th edn., CRC Press, Boca Raton, ISBN 1498754295, 2016.

Heaton, T. J., Köhler, P., Butzin, M., Bard, E., Reimer, R. W., Austin, W. E. N., Ramsey, C. B., Grootes, P. M., Hughen, K. A., Kromer, B., Reimer, P. J., Adkins, J., Burke, A., Cook, M. S., Olsen, J., and Skinner, L. C.: Marine20 – The Marine Radiocar-

bon Age Calibration Curve (0–55 000 cal BP), Radiocarbon, 62, 779–820, https://doi.org/10.1017/RDC.2020.68, 2020.

Heineke, C., Niedermann, S., Hetzel, R., and Akal, C.: Surface exposure dating of Holocene basalt flows and cinder cones in the Kula volcanic field (Western Turkey) using cosmogenic ^{3}He and ^{10}Be, Quat. Geochronol., 34, 81–91, https://doi.org/10.1016/j.quageo.2016.04.004, 2016.

Higham, T. F. G., Barton, H., Turney, C. S. M., Barker, G., Ramsey, C. B., and Brock, F.: Radiocarbon dating of charcoal from tropical sequences: results from the Niah Great Cave, Sarawak, and their broader implications, J. Quat. Sci., 24, 189–197, https://doi.org/10.1002/jqs.1197, 2009.

Hippe, K.: Constraining processes of landscape change with combined in situ cosmogenic ^{14}C–^{10}Be analysis, Quaternary Sci. Rev., 173, 1–19, https://doi.org/10.1016/j.quascirev.2017.07.020, 2017.

Hogg, A. G., Wilson, C. J. N., Lowe, D. J., Turney, C. S. M., White, P., Lorrey, A. M., Manning, S. W., Palmer, J. G., Bury, S., Brown, J., Southon, J., and Petchey, F.: Wiggle-match radiocarbon dating of the Taupo eruption, Nat. Commun., 10, 4669, https://doi.org/10.1038/s41467-019-12532-8, 2019.

Hogg, A. G., Heaton, T. J., Hua, Q., Palmer, J. G., Turney, C. S., Southon, J., Bayliss, A., Blackwell, P. G., Boswijk, G., Ramsey, C. B., Pearson, C., Petchey, F., Reimer, P., Reimer, R., and Wacker, L.: SHCal20 Southern Hemisphere Calibration, 0–55 000 Years cal BP, Radiocarbon, 62, 759–778, https://doi.org/10.1017/RDC.2020.59, 2020.

Holdaway, R. N., Duffy, B., and Kennedy, B.: Evidence for magmatic carbon bias in ^{14}C dating of the Taupo and other major eruptions, Nat. Commun., 9, 4110, https://doi.org/10.1038/s41467-018-06357-0, 2018.

Holdaway, R. N., Duffy, B., and Kennedy, B.: Reply to "Wiggle-match radiocarbon dating of the Taupo eruption", Nat. Commun., 10, 4668, https://doi.org/10.1038/s41467-019-12491-0, 2019.

Huntley, D. J. and Lamothe, M.: Ubiquity of anomalous fading in K-feldspars and the measurement and correction for it in optical dating, Can. J. Earth Sci., 38, 1093–1106, https://doi.org/10.1139/e01-013, 2001.

Huntley, D. J. and Lian, O. B.: Some observations on tunnelling of trapped electrons in feldspars and their implications for optical dating, Quat. Sci. Rev., 25, 2503–2512, https://doi.org/10.1016/j.quascirev.2005.05.011, 2006.

Huntley, D. J., Godfrey-Smith, D. I., and Thewalt, M. L. W.: Optical dating of sediments, Nature, 313, 105–107, https://doi.org/10.1038/313105a0, 1985.

Huntley, D. J., Hutton, J. T., and Prescott, J. R.: The stranded beach-dune sequence of south-east South Australia: A test of thermoluminescence dating, 0–800 ka, Quat. Sci. Rev., 12, 1–20, https://doi.org/10.1016/0277-3791(93)90045-N, 1993.

Hütt, G., Jaek, I., and Tchonka, J.: Optical dating: K-feldspars optical response stimulation spectra, Quaternary Sci. Rev., 7, 381–385, https://doi.org/10.1016/0277-3791(88)90033-9, 1988.

Ives, R. L.: Dating of the 1746 Eruption of Tres Virgenes Volcano, Baja California del Sur, Mexico, GSA Bull., 73, 647–648, https://doi.org/10.1130/0016-7606(1962)73[647:DOTEOT]2.0.CO;2, 1962.

Ivy-Ochs, S. and Kober, F.: Surface exposure dating with cosmogenic nuclides, E&G Quaternary Sci. J., 57, 179–209, https://doi.org/10.3285/eg.57.1-2.7, 2008.

Ivy-Ochs, S., Poschinger, A. v., Synal, H.-A., and Maisch, M.: Surface exposure dating of the Flims landslide, Graubünden, Switzerland, Geomorphology, 103, 104–112, https://doi.org/10.1016/j.geomorph.2007.10.024, 2009.

Jacobsson, P., Hamilton, W. D., Cook, G., Crone, A., Dunbar, E., Kinch, H., Naysmith, P., Tripney, B., and Xu, S.: Refining the Hallstatt Plateau: Short-Term 14C Variability and Small Scale Offsets in 50 Consecutive Single Tree-Rings from Southwest Scotland Dendro-Dated to 510–460 BC, Radiocarbon, 60, 219–237, https://doi.org/10.1017/RDC.2017.90, 2018.

Juvigné, É. and Gewelt, M.: La Narse d'Ampoix comme téphrostratotype dans la Chaîne des Puys méridionale (France), Quaternaire, 24, 37–48, https://doi.org/10.3406/quate.1987.1830, 1987.

Juvigné, E., Bastin, B., Delibrias, G., Evin, J., Gewelt, M., Gilot, E., and Streel, M.: A comprehensive pollen- and tephra-based chronostratigraphic model for the Late Glacial and Holocene period in the French Massif Central, Quat. Int., 34–36, 113–120, https://doi.org/10.1016/1040-6182(95)00075-5, 1996.

Kars, R., Wallinga, J., and Cohen, K.: A new approach towards anomalous fading correction for feldspar IRSL dating – tests on samples in field saturation, Radiat. Meas., 43, 786–790, https://doi.org/10.1016/j.radmeas.2008.01.021, 2008.

Kelley, S.: K–Ar and Ar–Ar Dating, Rev. Mineral. Geochem., 47, 785–818, https://doi.org/10.2138/rmg.2002.47.17, 2002.

Kigoshi, K.: Ionium Dating of Igneous Rocks, Science, https://doi.org/10.1126/science.156.3777.932, 1967.

Lacourse, T. and Gajewski, K.: Current practices in building and reporting age-depth models, Quat. Res., 96, 28–38, https://doi.org/10.1017/qua.2020.47, 2020.

Lakatos, S. and Miller, D. S.: Fission-track stability in volcanic glass of different water contents, J. Geophys. Res., 77, 6990–6993, https://doi.org/10.1029/JB077i035p06990, 1972.

Lal, D.: The present scope of the field of terrestrial cosmogenic nuclides, Curr. Sci., 61, 744–751, http://www.jstor.org/stable/24095301 (last access: 6 August 2024), 1991.

Lane, C. S., Brauer, A., Blockley, S. P. E., and Dulski, P.: Volcanic ash reveals time-transgressive abrupt climate change during the Younger Dryas, Geology, 41, 1251–1254, https://doi.org/10.1130/G34867.1, 2013.

Lane, C. S., Brauer, A., Martín-Puertas, C., Blockley, S. P. E., Smith, V. C., and Tomlinson, E. L.: The Late Quaternary tephrostratigraphy of annually laminated sediments from Meerfelder Maar, Germany, Quat. Sci. Rev., 122, 192–206, https://doi.org/10.1016/j.quascirev.2015.05.025, 2015.

Lane, C. S., Lowe, D. J., Blockley, S. P. E., Suzuki, T., and Smith, V. C.: Advancing tephrochronology as a global dating tool: Applications in volcanology, archaeology, and palaeoclimatic research, Quat. Geochronol., 40, 1–7, https://doi.org/10.1016/j.quageo.2017.04.003, 2017.

Laundal, K. M., Cnossen, I., Milan, S. E., Haaland, S. E., Coxon, J., Pedatella, N. M., Förster, M., and Reistad, J. P.: North–South Asymmetries in Earth's Magnetic Field, Space Sci. Rev., 206, 225–257, https://doi.org/10.1007/s11214-016-0273-0, 2017.

Le Corvec, N., Spörli, K. B., Rowland, J., and Lindsay, J.: Spatial distribution and alignments of volcanic centers: Clues to the formation of monogenetic volcanic fields, Earth Sci. Rev., 124, 96–114, https://doi.org/10.1016/j.earscirev.2013.05.005, 2013.

Lerner, G. A., Piispa, E. J., Bowles, J. A., and Ort, M. H.: Paleomagnetism and rock magnetism as tools for volcanology, Bull.

Volcanol., 84, 24, https://doi.org/10.1007/s00445-022-01529-9, 2022.

Li, B. and Li, S.-H.: Luminescence dating of K-feldspar from sediments: A protocol without anomalous fading correction, Quat. Geochronol., 6, 468–479, https://doi.org/10.1016/j.quageo.2011.05.001, 2011.

Li, B. and Li, S.-H.: Luminescence dating of Chinese loess beyond 130 ka using the non-fading signal from K-feldspar, Quat. Geochronol., 10, 24–31, https://doi.org/10.1016/j.quageo.2011.12.005, 2012.

Libby, W. F., Anderson, E. C., and Arnold, J. R.: Age Determination by Radiocarbon Content: World-Wide Assay of Natural Radiocarbon, Science, 109, 227–228, https://doi.org/10.1126/science.109.2827.227, 1949.

Lifton, N., Sato, T., and Dunai, T. J.: Scaling in situ cosmogenic nuclide production rates using analytical approximations to atmospheric cosmic-ray fluxes, Earth Planet. Sci. Lett., 386, 149–160, https://doi.org/10.1016/j.epsl.2013.10.052, 2014.

Linick, T. W., Damon, P. E., Donahue, D. J., and Jull, A. J. T.: Accelerator mass spectrometry: The new revolution in radiocarbon dating, Quat. Int., 1, 1–6, https://doi.org/10.1016/1040-6182(89)90004-9, 1989.

Lockwood, J. P. and Lipman, P. W.: Recovery of datable charcoal beneath young lavas: Lessons from Hawaii, Bull. Volcanol., 43, 609–615, https://doi.org/10.1007/BF02597697, 1980.

Lougheed, B. C., Obrochta, S. P., Lenz, C., Mellström, A., Metcalfe, B., Muscheler, R., Reinholdsson, M., Snowball, I., and Zillén, L.: Bulk sediment ^{14}C dating in an estuarine environment: How accurate can it be?, PALO, 32, 123–131, https://doi.org/10.1002/2016PA002960, 2017.

Lowe, D. J.: Tephrochronology and its application: A review, Quat. Geochronol., 6, 107–153, https://doi.org/10.1016/j.quageo.2010.08.003, 2011.

MacDonald, G. M., Beukens, R. P., Kieser, W. E., and Vitt, D. H.: Comparative radiocarbon dating of terrestrial plant macrofossils and aquatic moss from the "ice-free corridor" of western Canada, Geology, 15, 837–840, https://doi.org/10.1130/0091-7613(1987)15<837:CRDOTP>2.0.CO;2, 1987.

Mahan, S. A. and DeWitt, R.: Principles and history of luminescence dating, in: Handbook of Luminescence Dating, edited by: Bateman, M., Whittles Publishing, ISBN 978-1-84995-395-5, 2019.

Mahan, S. A., Rittenour, T. M., Nelson, M. S., Ataee, N., Brown, N., DeWitt, R., Durcan, J., Evans, M., Feathers, J., Frouin, M., Guérin, G., Heydari, M., Huot, S., Jain, M., Keen-Zebert, A., Li, B., López, G. I., Neudorf, C., Porat, N., Rodrigues, K., Sawakuchi, A. O., Spencer, J. Q. G., and Thomsen, K.: Guide for interpreting and reporting luminescence dating results, Geol. Soc. Am. Bull., 135, 1480–1502, https://doi.org/10.1130/B36404.1, 2022.

Malaguti, A. B., Rosi, M., Pistolesi, M., Speranza, F., and Menzies, M.: The contribution of palaeomagnetism, tephrochronology and radiocarbon dating to refine the last 1100 years of eruptive activity at Vulcano (Italy), Bull. Volcanol., 84, 12, https://doi.org/10.1007/s00445-021-01515-7, 2022.

Mangerud, J.: Radiocarbon dating of marine shells, including a discussion of apparent age of Recent shells from Norway, Boreas, 1, 143–172, https://doi.org/10.1111/j.1502-3885.1972.tb00147.x, 1972.

Manning, S. W.: Second Intermediate Period date for the Thera (Santorini) eruption and historical implications, PLOS ONE, 17, e0274835, https://doi.org/10.1371/journal.pone.0274835, 2022.

Manning, S. W., Kromer, B., Cremaschi, M., Dee, M. W., Friedrich, R., Griggs, C., and Hadden, C. S.: Mediterranean radiocarbon offsets and calendar dates for prehistory, Sci. Adv., 6, eaaz1096, https://doi.org/10.1126/sciadv.aaz1096, 2020.

Marinatos, S.: The Volcanic Destruction of Minoan Crete, Antiquity, 13, 425–439, https://doi.org/10.1017/S0003598X00028088, 1939.

Marsden, R. C., Danišík, M., Ahn, U. S., Friedrichs, B., Schmitt, A. K., Kirkland, C. L., McDonald, B. J., and Evans, N. J.: Zircon double-dating of Quaternary eruptions on Jeju Island, South Korea, J. Volcanol. Geoth. Res., 410, 107171, https://doi.org/10.1016/j.jvolgeores.2020.107171, 2021.

Martin, L. C. P., Blard, P.-H., Balco, G., Lavé, J., Delunel, R., Lifton, N., and Laurent, V.: The CREp program and the ICE-D production rate calibration database: A fully parameterizable and updated online tool to compute cosmic-ray exposure ages, Quat. Geochronol., 38, 25–49, https://doi.org/10.1016/j.quageo.2016.11.006, 2017.

Matchan, E. and Phillips, D.: New ^{40}Ar / ^{39}Ar ages for selected young (< 1 Ma) basalt flows of the Newer Volcanic Province, southeastern Australia, Quat. Geochronol., 6, 356–368, https://doi.org/10.1016/j.quageo.2011.03.002, 2011.

Matsu'ura, T., Miyagi, I., and Furusawa, A.: Late Quaternary cryptotephra detection and correlation in loess in northeastern Japan using cummingtonite geochemistry, Quat. Res., 75, 624–635, https://doi.org/10.1016/j.yqres.2010.12.004, 2011.

May, V. R., Chivas, A. R., Dosseto, A., Honda, M., Matchan, E. L., Phillips, D., and Price, D. M.: Quaternary volcanic evolution in the continental back-arc of southern Mendoza, Argentina, J. South Am. Earth Sci., 84, 88–103, https://doi.org/10.1016/j.jsames.2018.02.007, 2018.

McCreary, W.: Revisiting the volcanic sequence and age of the Puy de Lemptegy – Puy des Gouttes – Puy Chopine system in the Chaine des Puys, unpublished MS thesis, University of Freiburg, Freiburg, Germany, 106 pp., 2020.

McDougall, I. and Gill, E.: Potassium-Argon ages from the Quaternary succession in the Warrnambool-Port Fairy area, Victoria, Australia, Proc. Roy. Soc. Vic., 87, 175–178, 1975.

McDougall, I. and Harrison, T. M.: Geochronology and Thermochronology by the ^{40}Ar / ^{39}Ar Method, Oxford University Press, USA, New York, Oxford, 269 pp., https://doi.org/10.1093/oso/9780195109207.001.0001, 1999.

McNichol, A. P. and Lindauer, S.: Radiocarbon in the Marine Environment: An Overview, Radiocarbon, 64, 673–674, https://doi.org/10.1017/RDC.2022.16, 2022.

Merrihue, C.: Trace-element determinations and potassium-argon dating by mass spectroscopy of neutron-irradiated samples, Eos, 46, 125, 1965.

Merrihue, C. and Turner, G.: Potassium-argon dating by activation with fast neutrons, J. Geophys. Res., 71, 2852–2857, https://doi.org/10.1029/JZ071i011p02852, 1966.

Miallier, D., Fain, J., Sanzelle, S., Daugas, J., and Raynal, J.: Dating of the Butte de Clermont basaltic maar by means of the quartz inclusion method, PACT, 487–498, https://in2p3.hal.science/in2p3-00005490 (last access: 22 September 2025), 1982.

Millard, A. R.: Conventions for Reporting Radiocarbon Determinations, Radiocarbon, 56, 555–559, https://doi.org/10.2458/56.17455, 2014.

Mitchell, J.: The argon-40/argon-39 method for potassium-argon age determination, Geochim. Cosmochim. Acta, 32, 781–790, https://doi.org/10.1016/0016-7037(68)90012-4, 1968.

Muller, R. A.: Radioisotope Dating with a Cyclotron, Science, 196, 489–494, https://doi.org/10.1126/science.196.4289.489, 1977.

Murray, A., Roberts, R., and Wintle, A.: Equivalent dose measurement using a single aliquot of quartz, Radiat. Meas., 27, 171–184, https://doi.org/10.1016/S1350-4487(96)00130-8, 1997.

Murray, A. S. and Wintle, A. G.: Luminescence dating of quartz using an improved single-aliquot regenerative-dose protocol, Radiat. Meas., 32, 57–73, https://doi.org/10.1016/S1350-4487(99)00253-X, 2000.

Murray, A. S., Olley, J. M., and Caitcheon, G. G.: Measurement of equivalent doses in quartz from contemporary water-lain sediments using optically stimulated luminescence, Quaternary Sci. Rev., 14, 365–371, https://doi.org/10.1016/0277-3791(95)00030-5, 1995.

Nemeth, K.: Monogenetic volcanic fields: Origin, sedimentary record, and relationship with polygenetic volcanism, in: What is a Volcano?, edited by: Cañon-Tapia, E. and Szakács, A., Geological Society of America, vol. 470, 43–66, https://doi.org/10.1130/2010.2470(04), 2010.

Niedermann, S.: Cosmic-Ray-Produced Noble Gases in Terrestrial Rocks: Dating Tools for Surface Processes, Rev. Mineral. Geochem., 47, 731–784, https://doi.org/10.2138/rmg.2002.47.16, 2002.

Nier, A. O.: A redetermination of the relative abundances of the isotopes of carbon, nitrogen, oxygen, argon, and potassium, Phys. Rev., 77, 789, https://doi.org/10.1103/PhysRev.77.789, 1950.

Obrochta, S. P., Yokoyama, Y., Yoshimoto, M., Yamamoto, S., Miyairi, Y., Nagano, G., Nakamura, A., Tsunematsu, K., Lamair, L., Hubert-Ferrari, A., Lougheed, B. C., Hokanishi, A., Yasuda, A., Heyvaert, V. M. A., De Batist, M., and Fujiwara, O.: Mt. Fuji Holocene eruption history reconstructed from proximal lake sediments and high-density radiocarbon dating, Quaternary Sci. Rev., 200, 395–405, https://doi.org/10.1016/j.quascirev.2018.09.001, 2018.

Olley, J. M., Caitcheon, G. G., and Roberts, R. G.: The origin of dose distributions in fluvial sediments, and the prospect of dating single grains from fluvial deposits using optically stimulated luminescence, Radiat. Meas., 30, 207–217, https://doi.org/10.1016/S1350-4487(99)00040-2, 1999.

Ort, M. H., Porreca, M., and Geissman, J. W.: The use of palaeomagnetism and rock magnetism to understand volcanic processes: introduction, Geol. Soc. Lond. Spec. Publ., 396, 1–11, https://doi.org/10.1144/SP396.17, 2015.

Pearson, C., Sbonias, K., Tzachili, I., and Heaton, T. J.: Olive shrub buried on Therasia supports a mid-16th century BCE date for the Thera eruption, Sci. Rep., 13, 6994, https://doi.org/10.1038/s41598-023-33696-w, 2023.

Pearson, C. L., Brewer, P. W., Brown, D., Heaton, T. J., Hodgins, G. W. L., Jull, A. J. T., Lange, T., and Salzer, M. W.: Annual radiocarbon record indicates 16th century BCE date for the Thera eruption, Sci. Adv., 4, eaar8241, https://doi.org/10.1126/sciadv.aar8241, 2018.

Philippsen, B.: The freshwater reservoir effect in radiocarbon dating, Herit. Sci., 1, 24, https://doi.org/10.1186/2050-7445-1-24, 2013.

Phillips, D. and Matchan, E. L.: Ultra-high precision $^{40}Ar/^{39}Ar$ ages for Fish Canyon Tuff and Alder Creek Rhyolite sanidine: New dating standards required?, Geochim. Cosmochim. Ac., 121, 229–239, https://doi.org/10.1016/j.gca.2013.07.003, 2013.

Phillips, D., Matchan, E. L., Honda, M., and Kuiper, K. F.: Astronomical calibration of $^{40}Ar/^{39}Ar$ reference minerals using high-precision, multi-collector (ARGUSVI) mass spectrometry, Geochim. Cosmochim. Ac., 196, 351–369, https://doi.org/10.1016/j.gca.2016.09.027, 2017.

Phillips, F. M.: Cosmogenic ^{36}Cl ages of Quaternary basalt flows in the Mojave Desert, California, USA, Geomorphology, 53, 199–208, https://doi.org/10.1016/S0169-555X(02)00328-8, 2003.

Pilleyre, T., Montret, M., Fain, J., Miallier, D., and Sanzelle, S.: Attempts at dating ancient volcanoes using the red TL of quartz, Quat. Sci. Rev., 11, 13–17, https://doi.org/10.1016/0277-3791(92)90036-8, 1992.

Plunkett, G., Coulter, S. E., Ponomareva, V. V., Blaauw, M., Klimaschewski, A., and Hammarlund, D.: Distal tephrochronology in volcanic regions: Challenges and insights from Kamchatkan lake sediments, Glob. Planet. Change, 134, 26–40, https://doi.org/10.1016/j.gloplacha.2015.04.006, 2015.

Ponomareva, V., Portnyagin, M., and Davies, S. M.: Tephra without Borders: Far-Reaching Clues into Past Explosive Eruptions, Front. Earth Sci., 3, https://doi.org/10.3389/feart.2015.00083, 2015.

Preusser, F., Rufer, D., and Schreurs, G.: Direct dating of Quaternary phreatic maar eruptions by luminescence methods, Geology, 39, 1135–1138, https://doi.org/10.1130/G32345.1, 2011.

Randall, J. T. and Wilkins, M. H. F.: The phosphorescence of various solids, Proc. R. Soc. Lond. A. Math. Phys. Sci., 184, 347–364, https://doi.org/10.1098/rspa.1945.0023, 1945.

Reimer, P. J., Austin, W. E. N., Bard, E., Bayliss, A., Blackwell, P. G., Bronk Ramsey, C., Butzin, M., Cheng, H., Edwards, R. L., Friedrich, M., Grootes, P. M., Guilderson, T. P., Hajdas, I., Heaton, T. J., Hogg, A. G., Hughen, K. A., Kromer, B., Manning, S. W., Muscheler, R., Palmer, J. G., Pearson, C., van der Plicht, J., Reimer, R. W., Richards, D. A., Scott, E. M., Southon, J. R., Turney, C. S. M., Wacker, L., Adolphi, F., Büntgen, U., Capano, M., Fahrni, S. M., Fogtmann-Schulz, A., Friedrich, R., Köhler, P., Kudsk, S., Miyake, F., Olsen, J., Reinig, F., Sakamoto, M., Sookdeo, A., and Talamo, S.: The IntCal20 Northern Hemisphere Radiocarbon Age Calibration Curve (0–55 cal kBP), Radiocarbon, 62, 725–757, https://doi.org/10.1017/RDC.2020.41, 2020.

Reiners, P. W., Spell, T. L., Nicolescu, S., and Zanetti, K. A.: Zircon (U–Th) / He thermochronometry: He diffusion and comparisons with $^{40}Ar/^{39}Ar$ dating, Geochim. Cosmochim. Ac., 68, 1857–1887, https://doi.org/10.1016/j.gca.2003.10.021, 2004.

Reinig, F., Wacker, L., Jöris, O., Oppenheimer, C., Guidobaldi, G., Nievergelt, D., Adolphi, F., Cherubini, P., Engels, S., Esper, J., Land, A., Lane, C., Pfanz, H., Remmele, S., Sigl, M., Sookdeo, A., and Büntgen, U.: Precise date for the Laacher See eruption synchronizes the Younger Dryas, Nature, 595, 66–69, https://doi.org/10.1038/s41586-021-03608-x, 2021.

Renne, P. R., Sharp, W. D., Deino, A. L., Orsi, G., and Civetta, L.: $^{40}Ar/^{39}Ar$ Dating into the Historical Realm: Calibra-

tion Against Pliny the Younger, Science, 277, 1279–1280, https://doi.org/10.1126/science.277.5330.1279, 1997.

Renne, P. R., Deino, A. L., Hames, W. E., Heizler, M. T., Hemming, S. R., Hodges, K. V., Koppers, A. A. P., Mark, D. F., Morgan, L. E., Phillips, D., Singer, B. S., Turrin, B. D., Villa, I. M., Villeneuve, M., and Wijbrans, J. R.: Data reporting norms for $^{40}Ar/^{39}Ar$ geochronology, Quat. Geochronol., 4, 346–352, https://doi.org/10.1016/j.quageo.2009.06.005, 2009.

Rhodes, E. J., Singarayer, J., Raynal, J.-P., Westaway, K. E., and Sbihi-Alaoui, F.-Z.: New age estimates for the Palaeolithic assemblages and Pleistocene succession of Casablanca, Morocco, Quat. Sci. Rev., 25, 2569–2585, https://doi.org/10.1016/j.quascirev.2005.09.010, 2006.

Ritner, R. and Moeller, N.: The Ahmose "Tempest Stela", Thera and Comparative Chronology, J. Near Eastern Stud., 73, 1–19, https://doi.org/10.1086/675069, 2014.

Robertson, G. B., Prescott, J. R., and Hutton, J.: Thermoluminescence dating of volcanic activity at Mount Gambier, South Australia, Transactions of the Royal Society of South Australia, vol. 120, 7–12, 1996.

Rufer, D., Gnos, E., Mettier, R., Preusser, F., and Schreurs, G.: Proposing new approaches for dating young volcanic eruptions by luminescence methods, Geochronometria, 39, 48–56, https://doi.org/10.2478/s13386-011-0049-y, 2012.

Rufer, D., Preusser, F., Schreurs, G., Gnos, E., and Berger, A.: Late Quaternary history of the Vakinankaratra volcanic field (central Madagascar): insights from luminescence dating of phreatomagmatic eruption deposits, Bull. Volcanol., 76, 1–20, https://doi.org/10.1007/s00445-014-0817-7, 2014.

Sanzelle, S., Pilleyre, Th., Miallier, D., Fain, J., and Ganzawa, Y.: Thermoluminescence dating of a tephra deposit of the "'Toya"' volcano (Hokkaido, Japan), France, technical report, Laboratoire de Physique Corpusculaire, Université Biaise Pascal, 2000.

Savelkouls, A., Dalton, H., and Phillips, D.: High-resolution $^{40}Ar/^{39}Ar$ geochronology of the Koobi Fora Tuff Complex, Turkana Basin: Implications for the hominin bearing strata of the Early Pleistocene (1.6–1.4 Ma), Quat. Geochronol., 91, 101713, https://doi.org/10.1016/j.quageo.2025.101713, 2026.

Scaillet, S. and Guillou, H.: A critical evaluation of young (near-zero) K–Ar ages, Earth Planet. Sci. Lett., 220, 265–275, https://doi.org/10.1016/S0012-821X(04)00069-X, 2004.

Schaen, A. J., Jicha, B. R., Hodges, K. V., Vermeesch, P., Stelten, M. E., Mercer, C. M., Phillips, D., Rivera, T. A., Jourdan, F., Matchan, E. L., Hemming, S. R., Morgan, L. E., Kelley, S. P., Cassata, W. S., Heizler, M. T., Vasconcelos, P. M., Benowitz, J. A., Koppers, A. A. P., Mark, D. F., Niespolo, E. M., Sprain, C. J., Hames, W. E., Kuiper, K. F., Turrin, B. D., Renne, P. R., Ross, J., Nomade, S., Guillou, H., Webb, L. E., Cohen, B. A., Calvert, A. T., Joyce, N., Ganerød, M., Wijbrans, J., Ishizuka, O., He, H., Ramirez, A., Pfänder, J. A., Lopez-Martínez, M., Qiu, H., and Singer, B. S.: Interpreting and reporting $^{40}Ar/^{39}Ar$ geochronologic data, GSA Bull., 133, 461–487, https://doi.org/10.1130/B35560.1, 2020.

Schimmelpfennig, I., Benedetti, L., Finkel, R., Pik, R., Blard, P.-H., Bourlès, D., Burnard, P., and Williams, A.: Sources of in-situ ^{36}Cl in basaltic rocks. Implications for calibration of production rates, Quat. Geochronol., 4, 441–461, https://doi.org/10.1016/j.quageo.2009.06.003, 2009.

Schimmelpfennig, I., Benedetti, L., Garreta, V., Pik, R., Blard, P.-H., Burnard, P., Bourlès, D., Finkel, R., Ammon, K., and Dunai, T.: Calibration of cosmogenic ^{36}Cl production rates from Ca and K spallation in lava flows from Mt. Etna (38° N, Italy) and Payun Matru (36° S, Argentina), Geochim. Cosmochim. Ac., 75, 2611–2632, https://doi.org/10.1016/j.gca.2011.02.013, 2011.

Schmidt, C., Schaarschmidt, M., Kolb, T., Büchel, G., Richter, D., and Zöller, L.: Luminescence dating of late Pleistocene eruptions in the Eifel Volcanic Field, Germany, J. Quat. Sci., 32, 628–638, https://doi.org/10.1002/jqs.2961, 2017a.

Schmidt, C., Tchouankoue, J. P., Nkouamen Nemzoue, P. N., Ayaba, F., Nformidah-Ndah, S. S., and Nformi Chifu, E.: New thermoluminescence age estimates for the Nyos maar eruption (Cameroon Volcanic Line), PLoS one, 12, e0178545, https://doi.org/10.1371/journal.pone.0178545, 2017b.

Schmitt, A. K.: Uranium Series Accessory Crystal Dating of Magmatic Processes, Annu. Rev. Earth Planet. Sci., 39, 321–349, https://doi.org/10.1146/annurev-earth-040610-133330, 2011.

Schmitt, A. K., Stockli, D. F., and Hausback, B. P.: Eruption and magma crystallisation ages of Las Tres Vírgenes (Baja California) constrained by combined $^{230}Th/^{238}U$ and (U–Th) / He dating of zircon, J. Volcanol. Geotherm. Res., 158, 281–295, https://doi.org/10.1016/j.jvolgeores.2006.07.005, 2006.

Schmitt, A. K., Danišík, M., Evans, N. J., Siebel, W., Kiemele, E., Aydin, F., and Harvey, J. C.: Acigöl rhyolite field, Central Anatolia (part 1): high-resolution dating of eruption episodes and zircon growth rates, Contrib. Mineral. Petrol., 162, 1215–1231, https://doi.org/10.1007/s00410-011-0648-x, 2011.

Schmitt, A. K., Martín, A., Stockli, D. F., Farley, K. A., and Lovera, O. M.: (U–Th) / He zircon and archaeological ages for a late prehistoric eruption in the Salton Trough (California, USA), Geology, 41, 7–10, https://doi.org/10.1130/G33634.1, 2013.

Schoene, B., Condon, D. J., Morgan, L., and McLean, N.: Precision and Accuracy in Geochronology, Elements, 9, 19–24, https://doi.org/10.2113/gselements.9.1.19, 2013.

Sheppard, P. R., Ort, M. H., Anderson, K. C., Elson, M. D., Vázquez-selem, L., Clemens, A. W., Little, N. C., and Speakman, R. J.: Multiple Dendrochronological Signals Indicate the Eruption of ParíCutin Volcano, Michoacán, Mexico, Tree-Ring Res., 64, 97–108, https://doi.org/10.3959/2008-3.1, 2008.

Shitaoka, Y., Miyoshi, M., Yamamoto, J., Shibata, T., Nagatomo, T., and Takemura, K.: Thermoluminescence age of quartz xenocrysts in basaltic lava from Oninomi monogenetic volcano, northern Kyushu, Japan, Geochronometria, 41, 30–35, https://doi.org/10.2478/s13386-013-0144-3, 2014.

Shore, J. S., Bartley, D. D., and Harkness, D. D.: Problems encountered with the ^{14}C dating of peat, Quat. Sci. Rev., 14, 373–383, https://doi.org/10.1016/0277-3791(95)00031-3, 1995.

Small, C. and Naumann, T.: The global distribution of human population and recent volcanism, Global Environmental Change Part B: Environmental Hazards, 3, 93–109, https://doi.org/10.3763/ehaz.2001.0309, 2001.

Smith, I. E. M. and Németh, K.: Source to surface model of monogenetic volcanism: a critical review, in: Monogenetic Volcanism, edited by: Németh, K., Carrasco-Núñez, G., Aranda-Gómez, J. J., and Smith, I. E. M., Geological Society of London, vol. 446, https://doi.org/10.1144/SP446.14, 2017.

Snee, L. W.: Argon thermochronology of mineral deposits; a review of analytical methods, formulations, and selected applications, Bulletin, USGS, https://doi.org/10.3133/b2194, 2002.

Spooner, N.: Optical dating: preliminary results on the anomalous fading of luminescence from feldspars, Quat. Sci. Rev., 11, 139–145, https://doi.org/10.1016/0277-3791(92)90055-D, 1992.

Stuiver, M. and Polach, H. A.: Discussion Reporting of 14C Data, Radiocarbon, 19, 355–363, https://doi.org/10.1017/S0033822200003672, 1977.

Stuiver, M., Kromer, B., Becker, B., and Ferguson, C. W.: Radiocarbon age calibration back to 13 300 years BP and the ^{14}C age matching of the German oak and US bristlecone pine chronologies, Radiocarbon, 28, 969–979, https://doi.org/10.1017/S0033822200060252, 1986a.

Stuiver, M., Pearson, G. W., and Braziunas, T.: Radiocarbon Age Calibration of Marine Samples Back to 9000 Cal Yr BP, Radiocarbon, 28, 980–1021, https://doi.org/10.1017/S0033822200060264, 1986b.

Taddeucci, A., Broecker, W. S., and Thurber, D. L.: ^{230}Th dating of volcanic rocks, Earth Planet. Sci. Lett., 3, 338–342, https://doi.org/10.1016/0012-821X(67)90056-8, 1967.

Talamo, S. and Richards, M.: A Comparison of Bone Pretreatment Methods for AMS Dating of Samples > 30 000 BP, Radiocarbon, 53, 443–449, https://doi.org/10.1017/S0033822200034573, 2011.

Thiel, C., Buylaert, J.-P., Murray, A., Terhorst, B., Hofer, I., Tsukamoto, S., and Frechen, M.: Luminescence dating of the Stratzing loess profile (Austria) – Testing the potential of an elevated temperature post-IR IRSL protocol, Quat. Int., 234, 23–31, https://doi.org/10.1016/j.quaint.2010.05.018, 2011.

Thomsen, K. J., Murray, A. S., Jain, M., and Bøtter-Jensen, L.: Laboratory fading rates of various luminescence signals from feldspar-rich sediment extracts, Radiat. Meas., 43, 1474–1486, https://doi.org/10.1016/j.radmeas.2006.07.008, 2008.

Tsukamoto, S.: Optical dating of sediments using feldspar, Encyclopedia of Quaternary Science, 1, 765–781, https://doi.org/10.1016/B978-0-323-99931-1.00254-3, 2025.

Tsukamoto, S., Murray, A., Huot, S., Watanuki, T., Denby, P., and Bøtter-Jensen, L.: Luminescence property of volcanic quartz and the use of red isothermal TL for dating tephras, Radiat. Meas., 42, 190–197, https://doi.org/10.1016/j.radmeas.2006.07.008, 2007.

Tsukamoto, S., Kataoka, K., Oguchi, T., Murray, A. S., and Komatsu, G.: Luminescence dating of scoria fall and lahar deposits from Somma–Vesuvius, Italy, Quat. Geochronol., 20, 39–50, https://doi.org/10.1016/j.quageo.2013.10.005, 2014.

Turner, G. and Cadogan, P. H.: Possible effects of ^{39}Ar recoil in ^{40}Ar–^{39}Ar dating, Lunar and Planetary Science Conference Proceedings, 2, 1601–1615, https://doi.org/10.1038/242513b0, 1974.

Turner, G., Cadogan, P., and Yonge, C.: Apollo 17 age determinations, Nature, 242, 513–515, https://doi.org/10.1038/242513b0, 1973.

Turner, S., Bourdon, B., and Gill, J.: Insights into Magma Genesis at Convergent Margins from U-series Isotopes, Rev. Mineral. Geochem., 52, 255–315, https://doi.org/10.2113/0520255, 2003.

Valentine, G. A. and Connor, C. B.: Basaltic Volcanic Fields, in: The Encyclopedia of Volcanoes, 2nd edn., edited by: Sigurdsson, H., Academic Press, Amsterdam, 423–439, https://doi.org/10.1016/B978-0-12-385938-9.00023-7, 2015.

Valentine, G. A., Briner, J. P., van Wyk de Vries, B., Macorps, É., and Gump, D.: ^{10}Be exposure ages for the Late Pleistocene Gour de Tazenat maar (Chaîne des Puys volcanic field, Auvergne, France), Quat. Geochronol., 50, 8–13, https://doi.org/10.1016/j.quageo.2018.11.002, 2019.

Valentine, G. A., Ort, M. H., and Cortés, J. A.: Quaternary basaltic volcanic fields of the American Southwest, Geosphere, 17, 2144–2171, https://doi.org/10.1130/GES02405.1, 2021.

van der Plicht, J. and Hogg, A.: A note on reporting radiocarbon, Quat. Geochronol., 1, 237–240, https://doi.org/10.1016/j.quageo.2006.07.001, 2006.

Villemant, B., Boudon, G., and Komorowski, J.-C.: U-series disequilibrium in arc magmas induced by water-magma interaction, Earth Planet. Sci. Lett., 140, 259–267, https://doi.org/10.1016/0012-821X(96)00035-0, 1996.

Visocekas, R.: Tunnelling radiative recombination in labradorite: its association with anomalous fading of thermoluminescence, Int. J. Radiat. Appl. Instrum. Part D, 10, 521–529, https://doi.org/10.1016/0735-245X(85)90053-5, 1985.

Visocekas, R., Tale, V., Zink, A., and Tale, I.: Trap spectroscopy and tunnelling luminescence in feldspars, Radiat. Meas., 29, 427–434, https://doi.org/10.1016/S1350-4487(98)00062-6, 1998.

Visocekas, R., Barthou, C., and Blanc, P.: Thermal quenching of far-red Fe^{3+} thermoluminescence of volcanic K-feldspars, Radiat. Meas., 61, 52–73, https://doi.org/10.1016/j.radmeas.2013.11.002, 2014.

Volpe, A. M. and Hammond, P. E.: 238U230Th226Ra disequilibria in young Mount St. Helens rocks: time constraint for magma formation and crystallisation, Earth Planet. Sci. Lett., 107, 475–486, https://doi.org/10.1016/0012-821X(91)90094-X, 1991.

von Blanckenburg, F. and Willenbring, J. K.: Cosmogenic Nuclides: Dates and Rates of Earth-Surface Change, Elements, 10, 341–346, https://doi.org/10.2113/gselements.10.5.341, 2014.

Vörös, F., van Wyk de Vries, B., Karátson, D., and Székely, B.: DTM-Based Morphometric Analysis of Scoria Cones of the Chaîne des Puys (France) – The Classic and a New Approach, Remote Sens., 13, 1983, https://doi.org/10.3390/rs13101983, 2021.

Vörös, F., van Wyk de Vries, B., Guilbaud, M.-N., Görüm, T., Karátson, D., and Székely, B.: DTM-Based Comparative Geomorphometric Analysis of Four Scoria Cone Areas – Suggestions for Additional Approaches, Remote Sens., 14, 6152, https://doi.org/10.3390/rs14236152, 2022.

Wastegård, S.: Late Quaternary tephrochronology of Sweden: a review, Quat. Int., 130, 49–62, https://doi.org/10.1016/j.quaint.2004.04.030, 2005.

Wintle, A.: Detailed study of a thermoluminescent mineral exhibiting anomalous fading, J. Lumin., 15, 385–393, https://doi.org/10.1016/0022-2313(77)90037-0, 1977.

Wintle, A. G.: Anomalous fading of thermoluminescence in mineral samples, Nature, 245, 143–144, https://doi.org/10.1038/245143a0, 1973.

Wintle, A. G. and Murray, A. S.: Towards the development of a preheat procedure for OSL dating of quartz, Radiat. Meas., 29, 81–94, https://doi.org/10.1016/S1350-4487(97)00228-X, 1998.

Wohlfarth, B., Skog, G., Possnert, G., and Holmquist, B.: Pitfalls in the AMS radiocarbon-dating of terrestrial macrofossils,

J. Quat. Sci., 13, 137–145, https://doi.org/10.1002/(SICI)1099-1417(199803/04)13:2<137::AID-JQS352>3.0.CO;2-6, 1998.

Wolf, R. A., Farley, K. A., and Kass, D. M.: Modeling of the temperature sensitivity of the apatite (U–Th) / He thermochronometer, Chem. Geol., 148, 105–114, https://doi.org/10.1016/S0009-2541(98)00024-2, 1998.

Wood, R.: From revolution to convention: the past, present and future of radiocarbon dating, J. Archaeol. Sci., 56, 61–72, https://doi.org/10.1016/j.jas.2015.02.019, 2015.

Yamada, R., Tagami, T., Nishimura, S., and Ito, H.: Annealing kinetics of fission tracks in zircon: an experimental study, Chem. Geol., 122, 249–258, https://doi.org/10.1016/0009-2541(95)00006-8, 1995.

Yamamoto, S., Miyairi, Y., Yokoyama, Y., Serisawa, Y., Suga, H., Ogawa, N. O., and Ohkouchi, N.: Compound-specific radiocarbon analysis of sedimentary fatty acids: Potential as a dating tool for lake sediments of Mt. Fuji volcanic region, Japan, Org. Geochem., 196, 104860, https://doi.org/10.1016/j.orggeochem.2024.104860, 2024.

Zens, J., Zeeden, C., Römer, W., Fuchs, M., Klasen, N., and Lehmkuhl, F.: The Eltville Tephra (Western Europe) age revised: Integrating stratigraphic and dating information from different Last Glacial loess localities, Palaeogeogr. Palaeoclimatol. Palaeoecol., 466, 240–251, https://doi.org/10.1016/j.palaeo.2016.11.033, 2017.

Zolitschka, B., Francus, P., Ojala, A. E. K., and Schimmelmann, A.: Varves in lake sediments – a review, Quat. Sci. Rev., 117, 1–41, https://doi.org/10.1016/j.quascirev.2015.03.019, 2015.

Zöller, L. and Blanchard, H.: The partial heat – longest plateau technique: Testing TL dating of Middle and Upper Quaternary volcanic eruptions in the Eifel Area, Germany, E&G Quaternary Sci. J., 58, 86–106, https://doi.org/10.3285/eg.58.1.05, 2009.

Zöller, L., Blanchard, H., and McCammon, C.: Can temperature assisted hydrostatic pressure reset the ambient TL of rocks? – A note on the TL of partially heated country rock from volcanic eruptions, Ancient TL, 27, 15–22, https://doi.org/10.26034/la.atl.2009.425, 2009.